Distribution Category:
Environmental Control Technology
and Earth Sciences (UC-11)

ANL--83-100-Pt.4

DE85 009659

ARGONNE NATIONAL LABORATORY
9700 South Cass Avenue
Argonne, Illinois 60439

ENVIRONMENTAL RESEARCH DIVISION* ANNUAL REPORT

Atmospheric Physics
January—December 1983

P. F. Gustafson, Acting Director
M. L. Wesely, Program Manager

December 1984

Preceding Report

ANL-82-65 Part IV January—December 1982

*The Radiological and Environmental Research (RER) Division (A. F. Stehney, Acting Director) became part of the Environmental Research (ER) Division on the latter's formation in May 1983.

FOREWORD

This collection of articles provides a sample of the research conducted in 1983 by the Atmospheric Physics Program of Argonne National Laboratory's Environmental Research Division. The majority of the research described deals with atmospheric physical processes, but there is a substantial component dealing with chemical processes as well. With the increased emphasis on issues involving the atmospheric behavior and deposition rates of acidifying substances, many of the articles address the transport, diffusion, or deposition of atmospheric sulfur and nitrogen compounds. Numerical modeling and experimental studies are parallel activities in the Program and draw upon each other for information and guidance. More thorough accounts of the research can be found in the peer-reviewed scientific literature and Argonne topical reports listed at the end of this document.

Experimental studies of the planetary boundary layer continued in 1983 with the Boundary Layer eXperiment (BLX83), coordinated by the University of Wisconsin and involving several other universities and laboratories. Our objective as part of the U. S. Environmental Protection Agency's cloud venting (VENTEX) investigations was to study the flow of air near and in fair-weather clouds, which coincided with the main BLX83 objective. For the U. S. Department of Energy's Atmospheric Studies in COmplex Terrain (ASCOT) program, we continued to analyze data from past experiments and prepared for a major experiment planned for 1984. The Argonne minisodar, described in the second article, was designed to study shallow drainage flows in ASCOT experiments.

Four articles in the middle of this report describe numerical modeling studies. Long-range transport and dispersion are the major subjects. One article on modeling of chemical reactions in cumulus clouds represents a new effort beginning for the Department of Energy program on PRocessing of Emissions by Clouds and Precipitation (PRECP). Work in 1983 was preliminary; and full-level effort is expected in FY 1985.

Most of the last few articles in this report are on dry deposition, which was the subject of a large amount of the research conducted by this group in 1983. A site was established on the grounds of Argonne National Laboratory to monitor air quality and local micrometeorological conditions, with the goal of providing facilities to develop and test methods to monitor dry deposition rates routinely.

ANL PARTICIPATION IN BLX83

R. L. Coulter, T. J. Martin, M. L. Wesely, D. R. Cook, R. L. Hart, A. W. Burnett*, and S. S. Fine*

The Boundary Layer eXperiment 1983 (BLX83) was a cooperative, multilaboratory effort designed to investigate interactions between cumulus clouds and the developing planetary boundary layer (PBL). The experiment, led by Drs. Roland B. Stull and Edwin W. Eloranta of the University of Wisconsin, was conducted near Chickasha, Oklahoma, from May 20 to June 18, 1983. This research coincided with efforts by Argonne National Laboratory to investigate cloud inflow properties such as those efforts begun during the Vertical Observations Involving Convective Exchange (VOICE) experiment in 1982 in central Illinois (Coulter et al. 1982). The BLX83 research provided a great deal of additional data pertinent to cloud inflow properties. In addition to Argonne, participants included the University of Wisconsin (lidar, upper air soundings, program management), the National Center for Atmospheric Research (aircraft, PAM II system), the National Severe Storms Laboratory (Doppler radar, local contacts), and the U. S. Air Force and U. S. Army (upper air soundings). Argonne personnel operated the Doppler sodar, tethersonde, surface flux instrumentation and a dual-camera time-lapse photography setup to monitor cloud position relative to sodar location. The relative placement of instruments around the primary field site is shown in Figure 1.

Daytime operations included continuous operation of the Doppler sodar in a bistatic mode during early morning hours and in a monostatic mode for measurement of vertical velocities during the thermally active part of the day. The surface fluxes of heat, momentum, water vapor, and sulfur were measured in good weather as continuously as possible. Tethersonde profiles of dry- and wet-bulb temperature, wind speed, and wind direction were obtained throughout the day, with most runs during morning hours when conditions changed most rapidly. When clouds were present or predicted, a photographic

---

*Undergraduate Research Participants, Division of Educational Programs from Aquinas College, Grand Rapids, MI, and the University of Pennsylvania, University Park, PA, respectively.

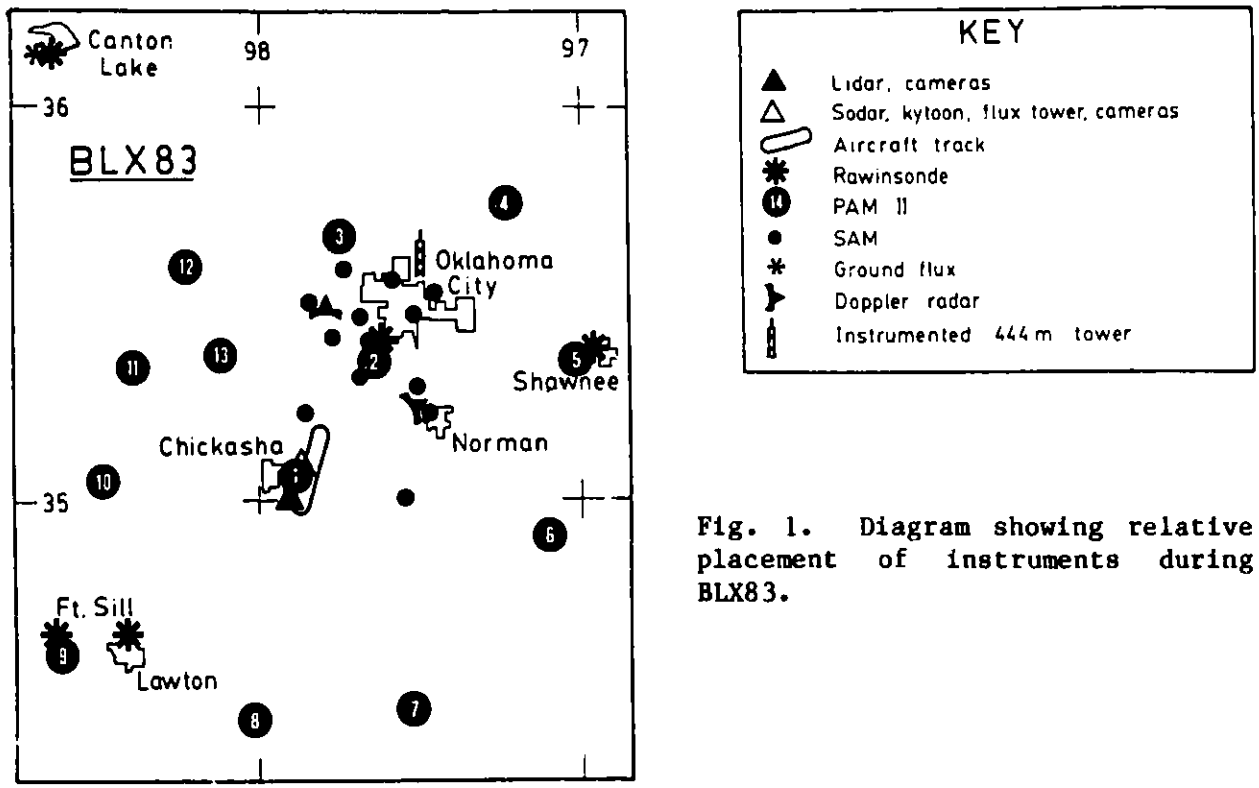

Fig. 1. Diagram showing relative placement of instruments during BLX83.

technique was used to map clouds. Two cameras were placed approximately 500 m from the sodar in positions such that baselines from the cameras to the sodar intersected at right angles at the sodar. Two cameras, which had 90-degree wide-angle lenses, were aimed vertically so that the minimum height of the intersection of the two fields of view was 500 m above the sodar. Cumulus clouds rarely formed below this height during the experiment. The cameras operated at periods from 33 to 262 s, depending on prevailing wind speeds and cloud heights. The University of Wisconsin lidar, located approximately 2.3 km SSW of the site operated by Argonne personnel, was pointed directly above the sodar and sensed PBL structure as depicted by scattering by aerosols. Tracking of aerosol inhomogeities at times allowed horizontal winds to be computed. A "picture" of the PBL structure over a horizontal scale near 10 km throughout the depth of the PBL could be obtained by varying the elevation and azimuth angles of the lidar. Since the lidar permits easy identification of clouds, the connections among the PBL vertical velocity field, the capping inversion, and cloud layers above could be made. Additionally, aircraft flew over the lidar and sodar sites at several altitudes to measure mean and turbulent statistics over long distances both near the surface and near cloud level.

Table 1. Times of operation of ANL sensors during BLX83 field study.

Date	Sodar	Surface Fluxes	Tethersonde	Cameras (period)
5-25	1000-2400	1530-2200		
5-26	0000-0830	1230-2400	1100-1300	1630-1800 (66 s)
	1100-2400		1600-1900	
5-27	0000-1800	0000-2330	0600-1530	1220-1845 (132 s)
5-28	0630-1700	0700-2030	0630-1630	
5-29	0600-1600	0700-2230	0630-1030	
		2145-2400		1500-1600
5-30				
5-31	0600-2400	1030-2400	0630-1130	1250-1845 (262 s)
6-1	0000-1930	0000-1700	0600-1130	1450-1640 (262 s)
			1430-1530	
6-2	0600-2400	0900-2400	0600-0700	1600-1650 (66 s)
			1000-1100	
6-3	0000-2400	0900-2400	0930-1030	2000-2400
6-4	0000-1730	0000-1630	0600-1100	2000-2400
	2000-2400			
6-5	0630-1500	0000-1500	0630-1000	
6-6	0900-2400	1130-2230		
6-7	0000-2400	0900-2400	0830-1030	1230-1530 (132 s)
			1300-1700	
6-8	0000-2400	0000-2400	0830-1130	1400-1810 (132 s)
			1500-1600	
6-9	0000-2400	0000-0430	0800-1030	1515-1840 (66 s)
	0800-2030			
6-10	0000-1530	1200-1830	0830-0930	1145-1220 (66 s)
6-11	1500-1800			
6-12	0800-2400	1000-2400	0830-0930	0940-1430 (33 s)
6-13	0000-1600	0000-1800		0940-1115 (33 s)
6-14	0900-2400		0930-1100	
			1400-1800	
6-15	0000-2400	1130-1800	0800-1030	
			1500-1600	
6-16	0000-1800	0800-1700	0730-1030	
			1600-1800	

*Times are Central Daylight.

The operation periods of Argonne sensors through the 24 days of participation are summarized in Table 1. A more complete compilation, including the activites of all BLX83 participants, is provided by Stull (1983). Sodar operation was almost continuous except for rainy periods and some nights when

severe weather was forecast. The camera system remained operational throughout the experimental period. Those days without camera operation were usually cloudless; other types of studies were undertaken on those days.

During several evenings and early mornings, tethersonde profiles and horizontal wind profiles derived from bistatic sodar operation were obtained for use in continuing studies of nocturnal profiles of wind and pollutants. In addition, ozone profiles at night and early morning were investigated with the tethersonde in conjunction with an NCAR aircraft being used to study nocturnal wind maxima as well as ozone distribution.

Detailed analyses of data for individual days and events within special time periods have not been completed. It appears that the ensemble of information is of good quality and promises to yield much insight into the interaction of the surface and well-mixed layers with the capping inversion and the cloud layer in the lower troposphere.

References

Coulter, R. L., T. J. Martin, and K. H. Underwood, 1982: The VOICE experiment--preliminary results, Radiological and Environmental Research Division Annual Report, ANL-82-65, Part IV, Argonne National Laboratory, pp. 1-6.

Stull, R. B. 1983: Boundary Layer Experiment-1983 Operations Log and Data Inventory, published by University of Wisconsin Meteorology Department, Madison, WI, 71 pp.

THE ARGONNE MINISODAR

R. L. Coulter, T. J. Martin, and F. T. DePaul

The Doppler sodar currently in use at Argonne operates at a frequency near 1300 Hz and uses a parabolic dish antenna. In this configuration the sodar can provide information about winds and thermal turbulence to altitudes near 1500 m. Its use is limited, however, to altitudes greater than 40 m by the response characteristics of the receiver antenna and the noncoincidence of the transmitter and receiver antenna beams in the bistatic configuration (Coulter and Martin 1980). To overcome this limitation, construction has begun on a high frequency sodar that can be used to probe the lower portions of the planetary boundary layer (PBL) and the surface layer of the atmosphere. The system being developed for use by Argonne will consist of a small phased-array antenna whose output and reception are controlled and analyzed by a microprocessor and fast digital signal processor, respectively.

The Argonne minisodar (so-named because of its relatively small size) is a compact, lightweight, portable system that will be capable of probing the lowest 100-200 m of the atmosphere. It will be capable of obtaining data from 10-300 m above the surface. Use of high frequencies (4-14 kHz) has several advantages. Because beamwidths are inversely proportional to both antenna size and frequency, the size of the antenna can be reduced while still maintaining a small beamwidth. With a reduction in antenna size comes a reduction in the size of the enclosure necessary to shield the antenna from ambient noise contamination. In addition, the amount of ambient noise present usually decreases with increasing frequency; thus the amount of shielding within the enclosure can also be reduced.

The use of higher frequencies also results in more accurate estimates of wind speed. The Doppler shift (d_f) of the received signal for monostatic geometries is given by

$$d_f = -2Vf/c, \tag{1}$$

where c is the speed of sound and V is wind speed. Thus, if Doppler shifts can be resolved to 1 Hz for all transmit frequencies considered, the

detectable velocity increment is decreased by the ratio of the old frequency to the new.

Balanced against these advantages is an attenuation coefficient that is about 15 times larger at 10 kHz than at 1 kHz. Because the reduction in signal increases exponentially with distance (height) and attenuation coefficient, the maximum range reached by a high-frequency system is severely limited.

Antenna design is very important for any sodar system. If a large number of small high-frequency speakers (tweeters) are spaced closely in a two-dimensional array and are operated in phase, a narrow beam pattern with a relatively large amount of output power can be obtained. The tweeters chosen for this first-generation Argonne device are approximately 5 cm in diameter, and are capable of 3 W electrical output. With 91 tweeters in a hexagonal, close-packed array in which every tweeter is surrounded by six others at equal distances, a beam pattern near 3 deg for one wavelength spacing is theoretically possible.

The calculated beam pattern for such an array is shown in Figure 1. Details of the pattern can be changed by choosing different array shapes, such as a square or diamond. The shape of the main peak around the pointing direction ($\phi = 0$), however, is governed principally by the number and spacing of the transmitters rather than by the perimeter shape. It is important, in addition, to look for locations in space that have local maxima. Figure 2 provides an example of contours of beam pattern strength (or sensitivity) at a constant radius from the center of the array. From this type of calculation, directions susceptible to ambient noise contamination can be defined. The calculations involved here have been made sufficiently general to allow many different spacings and patterns of transmitters to be evaluated. For example, by controlling individual tweeters, different beam patterns can be generated, and the effects of volume averaging can be investigated.

Because the tweeters are more efficient in converting electrical power to acoustic power than the transducers used in the low-frequency system, the amount of power put into the main beam of the array might be increased by a factor of three to ten. The precise values for beam width and power output will be determined when calibrations are performed.

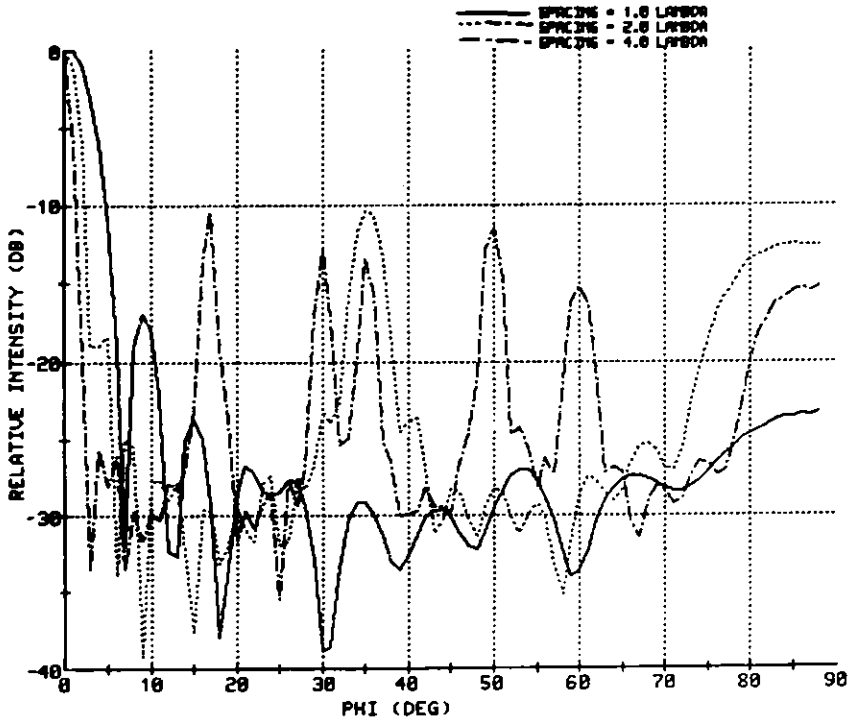

Fig. 1. Directivity of the antenna for different spacing between 91 individual tweeters in a hexagonal array. Phi (ϕ) is the angle from directly above the center of the array. Values are integrated over azimuth angles (θ).

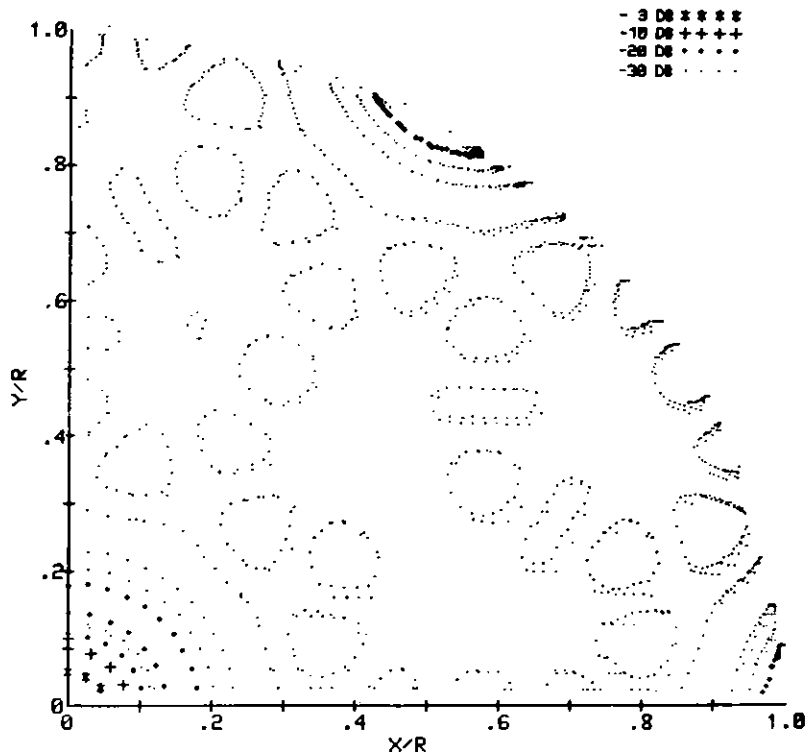

Fig. 2. Contours of relative sensitivity for a phased array-antenna consisting of 97 elements separated by one wavelength. Values are determined in the far field, at a constant distance from the center of the array. The field shown is a planar projection from a quarter of the hemispheric surface.

The minisodar system is intended for use in a Atmospheric Studies in COmplex Terrain (ASCOT) field study to be conducted in Colorado in September 1984 to study drainage flows. Because data will be limited to small ranges from the antenna, a pulse repetition rate of near 1 s^{-1} will be possible. This sampling rate will provide better data for the estimation both of means and variances in nonhomogeneous environments than would be provided at lower sampling rates.

Reference

Coulter, R. L. and T. J. Martin, 1980: Three-dimensional sodar capabilities, Radiological and Environmental Research Division Annual Report, ANL-80-115, Part IV, Argonne National Laboratory, pp. 11-14.

A METHOD FOR MEASURING MEAN WIND VELOCITIES IN A CANYON WITH TRACER BALLOONS

C. M. Sheih and B. J. Billman*

Measurements of entire wind velocity fields in confined areas not readily accessible can be a difficult task. For example, placement of in-situ sensing devices over a busy city street may interfere with traffic and pose safety problems. The utility of remote sensing devices, such as acoustic sounders, can be limited in confined areas by insufficient spatial resolution or by interference from background noise. A method developed to overcome these problems and measure mean wind velocity fields in such difficult environments is reported here. The method involves use of buoyant balloons as tracers. Sequential photographs of the balloons released at the ground level are taken with two cameras, and the wind velocity field is obtained by analyzing the balloon trajectories. An application of this method to studies of wind velocity distribution in an urban street canyon is reported elsewhere by DePaul and Sheih (1983). The purpose here is to summarize the methodology and the computational procedures.

The coordinate system used in defining the location of a tracer balloon in a street canyon of width L is shown in Figure 1. The coordinates x and z are in a vertical plane perpendicular to the coordinate y parallel to the street, where x and z are in the horizontal and the vertical direction, respectively. Two cameras, one at street level and the other at rooftop level, are used to take time-lapse photographs of the position B of the balloon. For convienence in analyzing photographic results, projected coordinates (x_o, y_o, z_o) of the balloon are determined first, and the actual balloon coordinates (x_B, y_B, z_B) are derived from the projected coordinates. The camera at street level (P in Figure 1) is used to determine x_o and z_o, which are the coordinates of the intersection point of the line-of-sight PB and the x-z plane. The camera at point Q at rooftop level is used to determine y_o, the intersection point of the line-of-sight QB and the vertical plane of the

*Undergraduate Research Participant, Division of Educational Programs, from the University of North Carolina, Raleigh, NC.

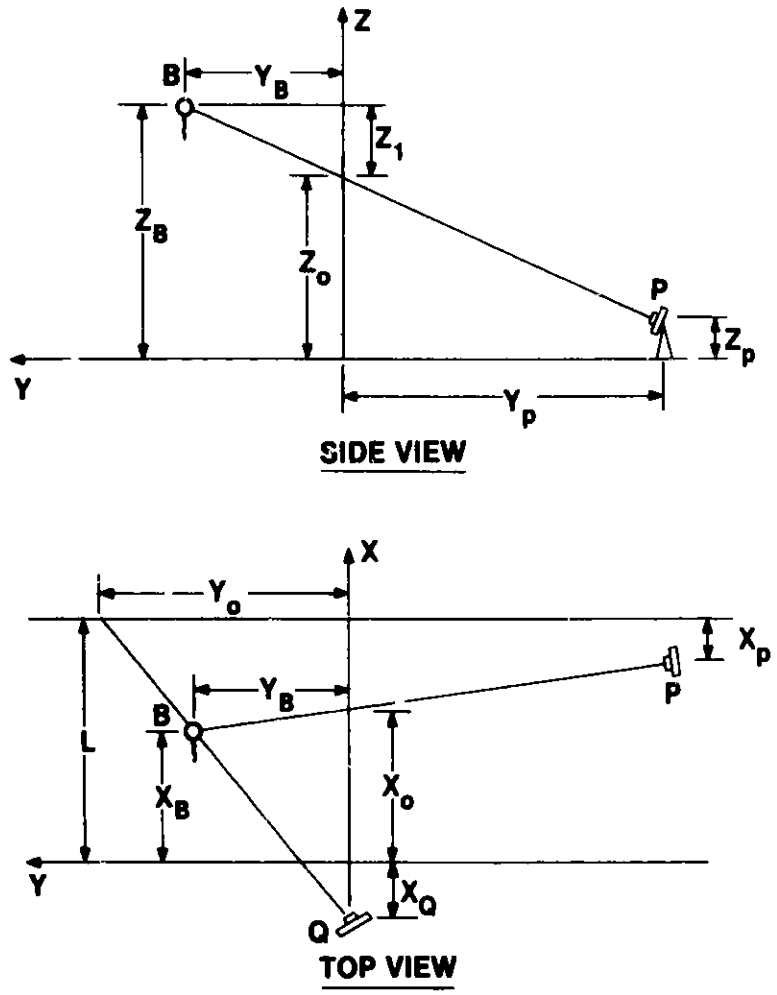

Fig. 1. The coordinate system of tracer balloon releases and tracking.

building wall at the opposite side of the camera site. Once the coordinates (x_o, y_o, z_o) are determined, the coordinates (x_B, y_B, z_B) of the balloon can be computed from the following relationships:

$$x_B = \left(\frac{x_p x_o}{x_o - L + x_p} + \frac{y_o x_Q}{L + x_p}\right) \left(\frac{y_p}{x_o - L + x_p} - \frac{y_o}{L + x_Q}\right)^{-1}, \quad (1)$$

$$y_B = \left(\frac{y_o}{L + x_Q}\right) (x_B + x_Q), \quad (2)$$

$$z_B = z_o + y_B (z_o - z_p)\, y^{-1}, \quad (3)$$

where x_p, y_p, z_p and x_Q are known variables determined from the locations of the two cameras shown in Figure 1.

The velocity components (u_B, v_B, w_B) of the tracer balloon are simply the time derivatives of (x_B, y_B, z_B). However, the buoyancy component of the balloon must be subtracted from w to obtain the true vertical wind velocity in the canyon. This buoyancy component may be estimated using the following procedure. If $w(x,y,z,t_i)$ is a true vertical wind velocity component at time t_i, $w_B(x,y,z,t_i)$ is the vertical velocity of the tracer balloon released at the time t_i , and $w_c(x,y,z,t_i)$ is the corresponding buoyancy velocity, then their relationship is:

$$w(x,y,z,t_i) = w_B(x,y,z,t_i) - w_c(x,y,z,t_i). \tag{4}$$

If the flow is assumed to be steady and the results of many balloons are averaged, time dependency will be eliminated, and Eq. (4) becomes

$$\bar{w}(x,y,z) = \frac{1}{N} \sum_{i=1}^{N} \left[w_B(z,y,z,t_i) - w_c(x,y,z,t_i)\right], \tag{5}$$

where N is the total number of balloons used in the computation. The first step to determine the mean buoyancy velocity is integrating Eq. (5) horizontally across the street canyon:

$$\int_o^L \bar{w}(x,y,z)dx = \int_o^L \frac{1}{N} \sum_{i=1}^{N} \left[(w_B(x,y,z,t_i) - w_c(x,y,z,t_i)\right]dx. \tag{6}$$

With the assumption that there is no convergence or divergence in the flow horizontally across the street, the left-hand side of Eq. (6) will be zero in order to satisfy the principle of mass conservation. With the additional assumptional that the buoyancy velocity averaged over all the balloons is independent of x, Eq. (6) can be rearranged to become:

$$\frac{1}{N} \sum_{i=1}^{N} w_c(x,y,z,t_i) = \frac{1}{L} \frac{1}{N} \int_o^L \sum_{i=1}^{N} w_B(x,y,z,t_i)dx. \tag{7}$$

Substitution of Eq. (7) into Eq. (5) yields:

$$\bar{w}(x,y,z) = \frac{1}{N} \sum_{i=1}^{N} w_B(x,y,z,t_i) - \frac{1}{L} \int_o^L \frac{1}{N} \sum_{i=1}^{N} w_B(x,y,z,t_i)dx. \tag{8}$$

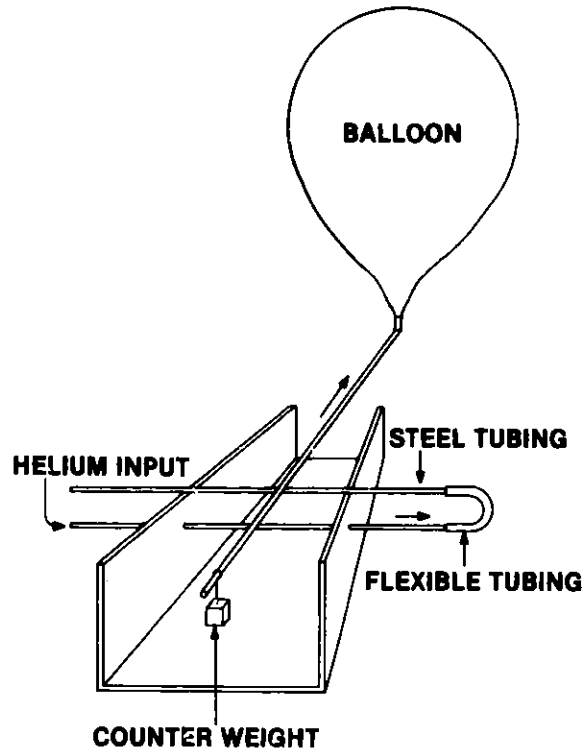

Fig. 2. The balloon filling system.

The second term of the right-hand side of Eq. (8) is a correction for buoyancy velocity of the balloon. Since no buoyancy correction is needed for the other two horizontal wind velocity components, their time averages are

$$\bar{u}(x,y,z) = \frac{1}{N} \sum_{i=1}^{N} u_B(x,y,z,t_i), \tag{9}$$

$$\bar{v}(x,y,z) = \frac{1}{N} \sum_{i=1}^{N} v_B(x,y,z,t_i). \tag{10}$$

If there is flow convergence or divergence, Eq. (7) is not valid, and the buoyancy component of the baloon velocity has to be measured directly. A simple setup for filling balloons to achieve a uniform buoyancy velocity is shown in Figure 2. The balloon is attached to one end of a balance made of brass tubing for passage of helium. An adjustable counterweight is attached to the other side of the balance arm for selecting an appropriate buoyancy force for the balloon. Once the location and the mass of the counterweight are determined for an appropriate buoyancy velocity, no further changes are made during the entire experiment. The balance arm is welded perpendicular to another piece of brass tubing that can freely rotate on the top of a U-shaped

support. One end of the tubing perpendicular to the balance arm is sealed, and the other end is connected to a small piece of very flexible rubber tubing that allows passage of helium for filling while minimizing the constraint to movement of the balance.

To evaluate the reproducibility of the system, a group of balloons then were inflated with helium to a diameter of approximately 0.5 m. Two balloons were then released simultaneously at ground level near a meteorological tower, and the rise times from the ground to the top of the tower (approximately 50 m) were measured. This procedure was repeated with a dozen sets of balloons. The results indicated that the buoyancy velocity of the balloon was reasonably reproducible. The difference between the rise time in each pair of balloons for a dozen releases was less than 2% of the average rise time to the 50 m height.

Reference

DePaul, F. T. and C. M. Sheih, 1983: Measurements of wind velocities in a street canyon. Atmos. Environ. (in press).

INDIRECT MEASUREMENTS OF TURBULENT FLUXES OVER THE SEA

P. Frenzen and R. L. Hart

A small experiment conducted during a research voyage in the North Atlantic in the spring of 1983* demonstrated that routine turbulent flux measurements could be made from a moving ship with relatively simple equipment. Fast-response cup anemometers of ANL design (Frenzen 1967; Wyngaard 1981) were used to record the variance of the fluctuating wind in a relatively high frequency band not affected by the wave-induced motions of the platform. The indirect high-frequency method (e.g., see Frenzen and Hart 1975; Large and Pond 1981) was then used to compute the momentum flux (i.e., the surface stress) from the Kolmogorov spectral relation and the turbulent energy equation.

In principle, vertical turbulent fluxes of any airborne passive additive (that is, any suspended material or atmospheric property that does not significantly affect the dynamics of the turbulent circulation) can be calculated in this way. During this project, efforts were also made to measure the fluxes of heat and moisture in addition to momentum. Unfortunately, the sensors (a fine-wire resistance thermometer and a Lyman-alpha hygrometer) could not be kept free of salt spray contamination. A much more effective ventilated housing designed to exclude water droplets will have to be developed before such measurements can be made at sea.

Experimental Arrangements

For these measurements over the open sea, a modified version of the ANL anemometer designed to survive the higher wind velocities was used. This sensor was mounted on a slender boom extending about 4 m above and 3 m forward of the ship's pilot house; signal conditioners were placed at the base of the foremast, and data processing equipment was located immediately below, in the

*Work performed aboard USNS Lynch enroute from Charleston, SC, to Los Palmas, Canary Islands, and Glasgow, Scotland, during a study of the marine boundary layer organized by the Naval Research Laboratory.

ship's chartroom. During operation, high-frequency wind signals in the selected frequency range (typically 3 to 9 Hz) were fed to a preprogramed microprocessor that computed the variance of the filtered signal. This unit also computed the mean value of the unfiltered signal and, on command, recorded selected runs for subsequent, independent spectral computation and analysis.

Results

A total of 340 runs, ranging from 7.5 to 30 minutes in duration, were recorded at various times throughout the voyage. No measurements were made when the winds were obviously too light, as was the case during much of the voyage south of 25 deg N. lat. These periods were largely spent in unsuccessful attempts to improve the performance of the humidity sensor. Sensible heat fluxes were almost always too small to provide an adequate test of the fine-wire thermometer, even if it could have been kept free of contamination.

Figures 1 and 2 illustrate one set of data obtained on Julian Day 101 (11 April). At this time, the ship was proceeding on a heading of 019 deg at a speed averaging 8.5 knots, on a course crossing the 35th parallel about 300 miles west of Gibraltar. True winds from 030-040 deg averaged 6 to 7 m s^{-1} during the first six hours. After 0600 Z, the wind veered to 055-065 deg and steadily accelerated (see Figure 1), reaching speeds of 10 to 12 m s^{-1} by midday before decreasing again in the evening. Except for short periods when operation was temporarily suspended, the data-processing equipment produced a turbulence dissipation estimate every 30 minutes. A notable exception appears at 1500 Z, when an interruption of the 30-minute routine by a 7.5-minute taped run evidently produced a statistically unrepresentative sample of the fluctuating wind.

Friction velocity (u_*) estimates calculated from the true wind speeds and a drag coefficient (using the relation suggested by Garratt 1977) were compared with those derived from the observed dissipation rates by the high-frequency variance method. This comparison effectively determines an estimate of z, the apparent height above the sea from which the turbulent eddies sensed by the anemometer must have come. For runs plotted in Figure 1 prior to 0600 Z, that height was only about 3 m; for runs after 0600 Z, the height averaged about 6 m. Since the anemometer was actually located 13.5 m above the sea, an

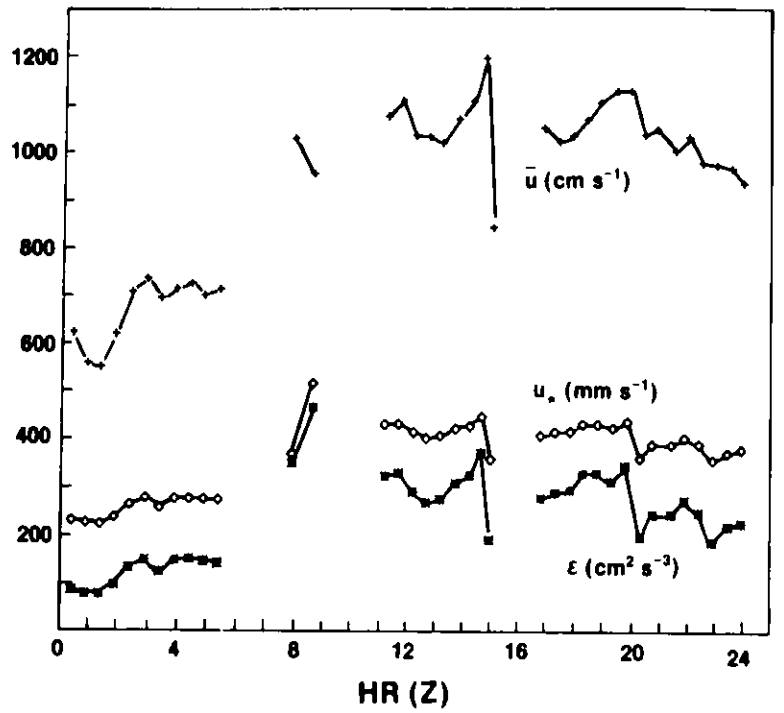

Fig. 1. True wind speeds ($\bar{u}$), friction velocities (u_*), and turbulence dissipation rates recorded on Julian Day 101, in units shown.

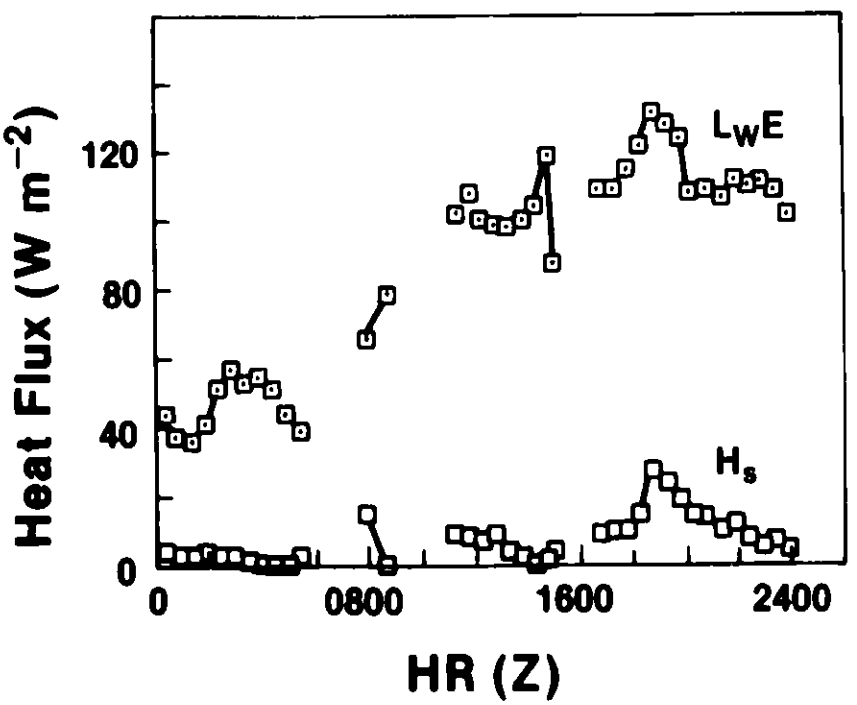

Fig. 2. Fluxes of sensible (H_s) and latent (L_wE) heat in W m^{-2} calculated for periods of runs on Julian Day 101.

apparent source elevation of only 3 m is surprisingly small. On the other hand, an elevation of 6 m is not, in view of the distortion of the wind field over the sea caused by a moving ship and the relatively unfavorable location of the anemometer during these measurements. Similar abrupt changes of this estimated height of origin were observed on a number of occasions. These could have been associated with stability transitions through neutrality, or with a flow transition between aerodynamically smooth and aerodynamically rough flow that can occur at wind speeds of 6-7 m s^{-1}. Individual effects of smooth and stable regimes are difficult to separate since, over the open sea, they apparently often occur simultaneously.

Values of sensible and latent heat flux determined by bulk aerodynamic methods and plotted in Figure 2 suggest that on Day 101 the stratification was always unstable: the Monin-Obukhov stability length L apparently remained negative throughout the period. However, a change in the apparent origin of the flow suggests that conditions prior to 0600 Z may have been stably stratified. A relatively small error in sea surface temperature could have accounted for both a reversal of the direction of the sensible heat flux and reduction in the magnitudes of both thermal energy fluxes sufficient to change the sign of the rate of turbulent energy production due to buoyancy, and hence in the stability parameter L. Since sea-surface temperatures were measured by the bucket method, errors of this kind were entirely possible.

Data obtained during this voyage are being made available to the other researchers aboard, many of whom were studying the nature of marine aerosol in the surface layer. Surface stress is one of several factors that contribute to the structure of aerosol specta at sea.

References

Frenzen, P., 1967: Modifications of cup anemometer design to improve the measurement of mean horizontal wind speeds in turbulence, Radiological Physics Division Annual Report, ANL-7360, Argonne National Laboratory, pp. 160-166.

Frenzen, P. and R. L. Hart, 1975: Wind stress and turbulence energy budget measurements in the undisturbed surface boundary layer over the sea, BOMEX Bull. 12, 79-86.

Garratt, J. R., 1977: Review of drag coefficients over oceans and continents, Mon. Wea. Rev. 105, 915-929.

Large, W. G. and S. Pond, 1981: Open ocean momentum flux measurements in moderate to strong winds, J. Phys. Oceanog. 11, 324-336.

Wyngaard, J. C., 1981: Cup, propeller, vane, and sonic anemometers in turbulence research, Ann Rev. Fluid Mech. 13, 399-423.

PHYSICAL AND CHEMICAL PROPERTIES OF CUMULUS CLOUDS

I.-Y. Lee

Dynamic and microphysical processes of clouds have been coupled with in-cloud chemical reactions in order to study cloud droplet and rainwater acidification processes associated with cumulus clouds. The in-cloud chemistry model (Table 1) in this study is a modification of previous work (Lee and Shannon 1984). In the present study, reactions associated with ozone and hydrogen peroxide are included. In Table 1, reactions 1 through 11 are assumed to be at equilibrium state, while kinetic computations are carried out for reactions 12 through 14. The water-soluble portion of aerosols is assumed to be composed of sulfuric acid, sulfate, and nitrate. At electro-neutrality, the hydrogen ion concentration in cloud and rainwater may be written as

$$\left(1 + \frac{KH_5K_6}{K_1} P_{HNO_3}\right) [H^+]^3 - \left(\frac{2000\ m_s\rho_w}{M_s\rho_a Q} + \frac{1000\ m_n\rho_w}{M_n\rho_a Q}\right) [H^+]^2$$

$$- \frac{1}{\gamma_+\gamma_-} \left(K_1 + KH_2K_3P_{SO_2} + KH_7K_8P_{CO_2} + KH_{10}K_{11}P_{HNO_3}\right) [H^+]$$

$$- \frac{1}{\gamma_+^2\gamma_=} \left(KH_2K_3K_4P_{SO_2} + KH_7K_8K_9P_{CO_2}\right) = 0 \qquad (1)$$

where K denotes the equilibrium constant, KH the Henry constant, P the gaseous pressure, m_s and m_n the sulfate and nitrate mass densities in air, M_s and M_n the molecular weight of sulfate and nitrate, and γ the activity coefficient. The cloud model, which is a version of that of Asai and Kasahara (1967) modified to include more microphysical properties, computes temporal changes for several variables. Included are dynamic variables such as vertical velocity, temperature, water vapor and liquid water mixing ratios, and chemical species concentrations in clouds as well as in clear regions. Aqueous chemical variables include such properties as pH values in cloud and rain water and ionic concentrations of chemical species involved in aqueous chemical reactions. Microphysical and chemical properties computed include spectral evolution and pH values for drops of different sizes.

Computations have been carried out with following initial conditions. In the subcloud layer, the temperature decreases dry adiabatically to 20 °C at

Table 1. In-cloud chemistry model.

	Reactions	Constants	Source
1.	$H_2O \leftrightarrow H^+ + OH^-$	$K_1 = 10^{-14}\ M^2$	Orel and Seinfeld (1977)
2.	$SO_2 + H_2O \leftrightarrow SO_2 \cdot H_2O$	$KH_2 = 1.24\ M\ atm^{-1}$	Orel and Seinfeld (1977)
3.	$SO_2 \cdot H_2O \leftrightarrow H^+ + HSO_3^-$	$K_3 = 0.022\ M$	Möller (1980)
4.	$HSO_3^- \leftrightarrow H^+ + SO_3^=$	$K_4 = 6.24 \times 10^{-8}\ M$	Orel and Seinfeld (1977)
5.	$NH_3 + H_2O \leftrightarrow NH_3 \cdot H_2O$	$KH_5 = 92.9\ M\ atm^{-1}$	Hales and Drewes (1979)
6.	$NH_3 \cdot H_2O \leftrightarrow NH_4^+ + OH^-$	$K_6 = 1.774 \times 10^{-5}\ M$	Orel and Seinfeld (1977)
7.	$CO_2 + H_2O \leftrightarrow CO_2 \cdot H_2O$	$KH_7 = 0.034\ M\ atm^{-1}$	Orel and Seinfeld (1977)
8.	$CO_2 \cdot H_2O \leftrightarrow H^+ + HCO_3^-$	$K_8 = 7.679 \times 10^{-7}\ M$	Adamowicz (1979)
9.	$HCO_3^- \leftrightarrow H^+ + CO_3^=$	$K_9 = 4.68 \times 10^{-11}\ M$	Orel and Seinfeld (1977)
10.	$HNO_3 + H_2O \leftrightarrow HNO_3 \cdot H_2O$	$KH_{10} = 2.1\ 10^5\ M\ atm^{-1}$	Davis and de Bruin (1964)
11.	$HNO_3 \cdot H_2O \leftrightarrow H^+ + NO_3^-$	$K_{11} = 15.4\ M$	Davis and de Bruin (1964)
12.	$d[SO_4^=]/dt = k_{12}[SO_3^=]$	$k_{12} = 0.003\ s^{-1}$	Miller and de Pena (1972)
13.	$d[SO_4^=]/dt = k_{13}KH_{13}[S(IV)]\ P_{O_3}$	$k_{13} = \exp(0.92\ pH + 9.8)\ M^{-1}\ s^{-1}$	Möller (1980)*
		$KH_{13} = 0.022\ M\ atm^{-1}$	
14.	$d[SO_4^=]/dt = k_{14}KH_{14}[S(IV)]\ P_{H_2O_2}$	$k_{14} = \exp(-0.74\ pH^2 + 6.378pH - 6.573)\ M^{-1}\ s^{-1}$	
		$KH_{14} = 5.041 \times 10^4\ M\ atm^{-1}$	Möller (1980)*

*The rate constants k_{13} and k_{14} are derived from data, and k_{14} is good when $4 < pH < 7$.

about 1000 m above the surface, and the relative humidity increases slowly to 95% at the same level. An inversion layer with its base at about 3000 m inhibits extensive convection. The region between subcloud and inversion layers, in which cloud formation and dissipation may occur, has a temperature lapse rate of about 7 °C km^{-1} and a water vapor mixing ratio decreasing by 2 to 5 g kg^{-1} km^{-1}. The initial aerosol is a modification of a continental background aerosol distribution. The total number density and the bulk density of aerosols are 1643 cm^{-3} and 1.8 g cm^{-3}, respectively, with mode at 0.08 μm radius. The soluble portion of aerosols is 70%, and the ratio of ammonium sulfate to total sulfate is 0.5. Initial values for SO_2, NH_3, HNO_3, O_3, and H_2O_2 are set to be 9.8, 2.0, 2.3, 20.0, and 1.0 ppb, respectively, and their vertical gradients are assumed to be zero. The ratio of cloudy to clear horizontal area coverage is set to be 0.1, and the air is assumed to be saturated in portions of the cloud region (1000 to 2000 m) initially.

Preliminary results are presented in Figures 1 through 7. Simulations of vertical velocity W (Figure 1), liquid water mixing ratio Q (Figure 2) and precipitation R (Figure 3) show the typical dynamic characteristics associated with cumulus clouds. The maximum values of both W and Q are located in the upper part of the cloud, with W about 3.5 m s^{-1} and Q about 1.2 g kg^{-1}. On the other hand, the maximum in-cloud precipitation rate of 2.5 mm h^{-1} occurs after 20 min of cloud development in the middle of the cloud. Development of virga occurs after about 15 min of real time simulation. Two trajectories are computed: one remains near the cloud base and the other passes through the middle of the cloud to the cloud top. Droplet spectral analyses have been made at selected locations along these trajectories. The temporal and spatial variations of in-cloud SO_2, ambient SO_2, and pH are presented in Figures 4 through 6. The in-cloud decrease in SO_2 concentration occurs mainly in the upper part of the cloud, with a maximum of about 85%; while the corresponding maximum SO_2 loss in the ambient air is about 22%. Our analysis shows that the SO_2 oxidation is increased by 50% because of the kinetic oxidation by H_2O_2. The reduction of the SO_2 concentration in the upper part of the cloud environment is due to modification by detrainment from the cloud. The amount of SO_2 uptake increases with the increase of the liquid water mixing ratio. The pH field shows a pattern similar to that of cloud water mixing ratio and ranges from 3.0 to 4.5. Our analysis shows that the response between the variations of dissolved SO_2 and of Q is nonlinear and that the dilution by Q

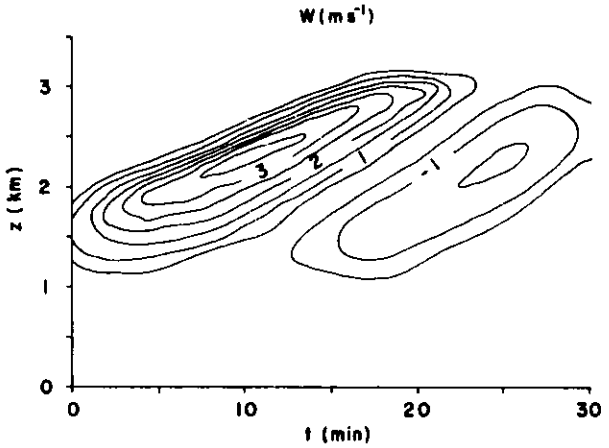

Fig. 1. Temporal and spatial variation of vertical velocity.

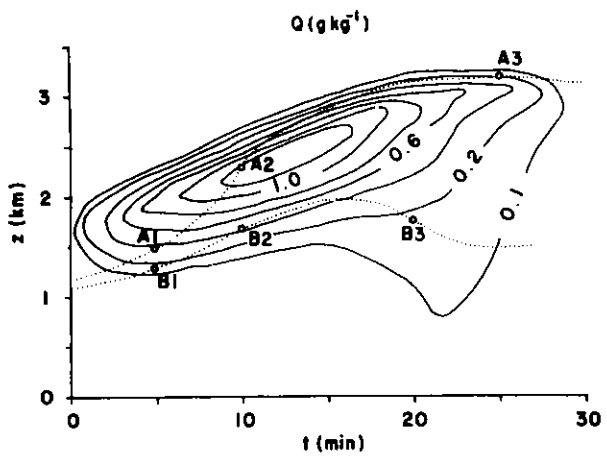

Fig. 2. Temporal and spatial variation of liquid water mixing ratio. (The dotted lines denote the air parcel trajectories.)

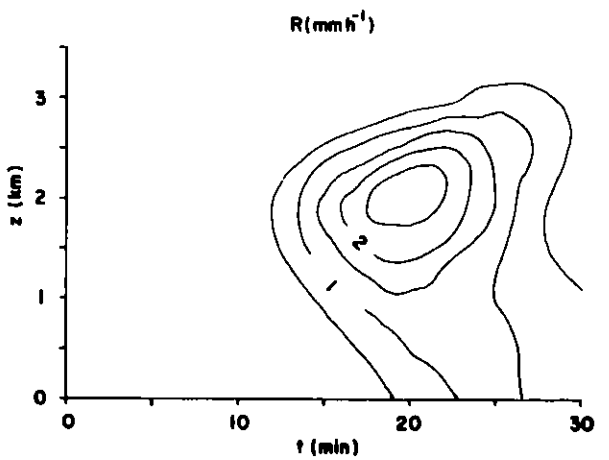

Fig. 3. Temporal and spatial variation of rainwater.

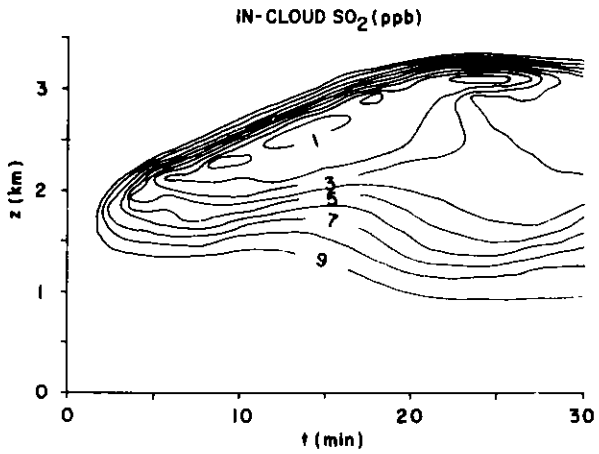

Fig. 4. Temporal and spatial variation of in-cloud sulfur dioxide.

Fig. 5. Temporal and spatial variation of ambient sulfur dioxide.

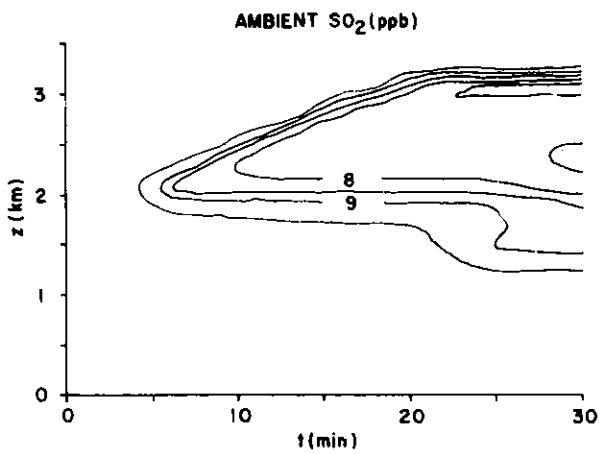

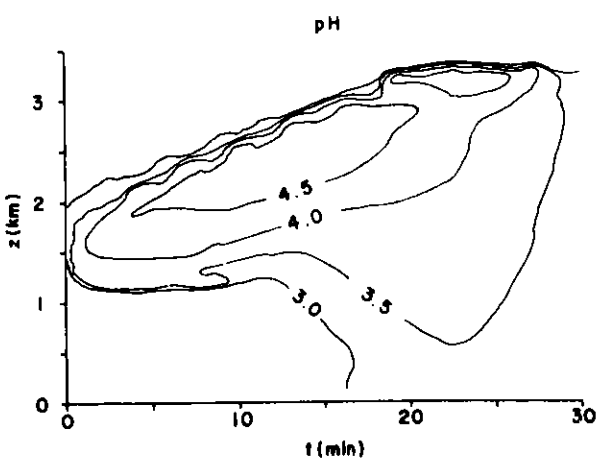

Fig. 6. Temporal and spatial variation of cloud and rainwater pH.

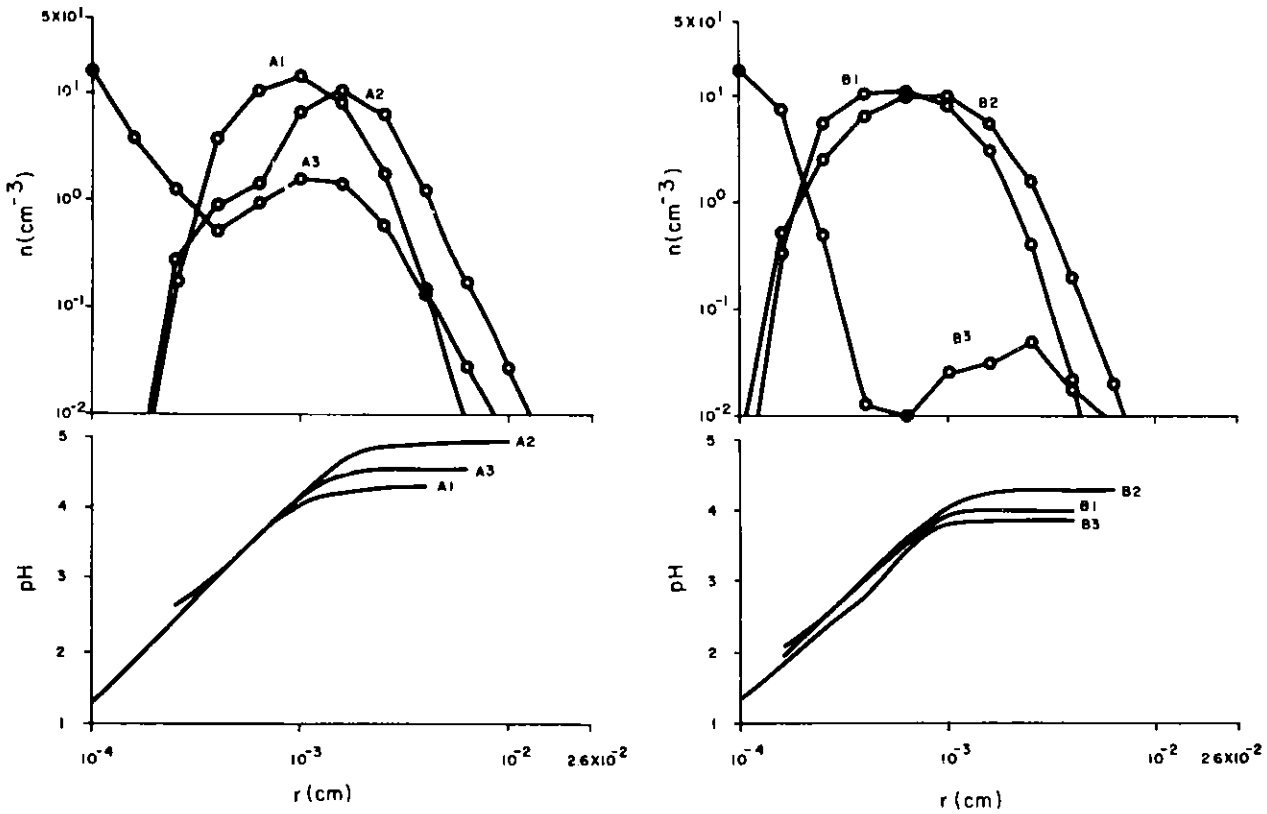

Fig. 7. Droplet spectral evolution and corresponding pH changes at (left) locations A1, A2, and A3; and (right) locations B1, B2, and B3 (see Figure 2).

overcompensates for the increase in uptake of acidifying species. Therefore, low acidity corresponds to high Q values and vice versa. The spectral evolution of cloud and raindrops and corresponding changes in droplet pH are presented (Figure 7) at selected locations as shown in Figure 2. In general, the mode size reaches a maximum where the Q value is high, a bimodal spectrum develops during the dissipation stage of the cloud cycle, and the pH ranges between 4 and 5 for drops larger than about 20 μm radius.

References

Adamowicz, R. F., 1979: A model for the reversible washout of sulphur dioxide, ammonia, and carbon dioxide from a polluted atmosphere and the production of sulphates in raindrops, Atmos. Environ. 13, 105-121.

Asai, T. and A. Kasahara, 1967: A theoretical study of the compensating downward motions associated with cumulus clouds, J. Atmos. Sci. 24, 487-496.

Davis, W., Jr., and H. J. de Bruin, 1964: New activity coefficients of 0-100 percent aqueous nitric acid, J. Inorg. Nucl. Chem. 26, 1069-1083.

Hales, J. M. and D. R. Drewes, 1979: Solubility of ammonia in water at low concentrations, Atmos. Environ. 13, 1133-1148.

Lee, I.-Y. and J. D. Shannon, 1984: Indications of nonlinearities in processes of wet deposition, Atmos. Environ. (in press).

Miller, J. M. and R. de Pena, 1972: Contribution of scavenged sulfur dioxide to the sulfate of rainwater, J. Geophys. Res. 30, 5905-5916.

Möller, D., 1980: Kinetic model of atmospheric SO_2 oxidation based on published data, Atmos. Environ. 14, 1067-1076.

Orel, A. E. and J. H. Seinfeld, 1977: Nitrate formation in atmospheric aerosols, Environ. Sci. Technol. 11, 1000-1007.

ESTIMATES OF SULFUR FLUXES OUT OF NORTH AMERICA

J. D. Shannon

There are three major mechanisms for removal of sulfur from the atmosphere over North America--deposition over the continent by wet processes, deposition by dry processes, or transport away from the continent for eventual deposition elsewhere. (Deposition by fog droplet collection or cloud impingement can be considered a special case of either wet or dry deposition.) When these three major "sinks" are estimated from numerical simulations, only wet deposition can be compared with routine direct observations, i.e., data from precipitation chemistry monitoring networks. A similar comparison with observations of dry deposition must await the development and deployment of dry deposition samplers, or the deployment of air quality monitors at well-characterized, regionally representative sites. Until recently there were no acceptable observations of net mass coastal flux of sulfur, but results of a study combining upper-air wind statistics with vertical profiles of average concentrations of oxides of sulfur and nitrogen near the Atlantic coast have become available (Galloway et al. 1984). The approach used in that study is as close to long-term monitoring of net coastal flux as is possible without a dedicated field sampling program.

Partly for an independent estimate and partly to check internal model consistency, the Advanced Statistical Trajectory Regional Air Pollution (ASTRAP) model (Shannon 1981) has been modified to calculate net sulfur flux past the same eight segments of the Atlantic coast as used by Galloway et al., plus the other external borders of the United States and Canada. A previous approach used to calculate horizontal net mass flux in ASTRAP simulations (Shannon 1979) was to define the area of interest by X limits on each Y column and Y limits on each X row, and to maintain a count of simulated tracers that go from inside to outside or vice versa during each time step. The total area of simulation was thus in one of two categories, inside the region of interest or outside the region. The approach here is slightly different; regularly spaced grid cells are coded to indicate location inside the region of interest or in one of 12 areas that consist of eight latitude bands east of the Atlantic Coast, the Gulf of Mexico, Mexico, the Pacific, and areas north of 60 deg N lat. plus Hudson Bay.

If a simulated tracer trajectory goes from the interior to one of the 12 outside areas, a counter identified by emission source cell, outside region, and plume age is incremented by the fraction of an initial unit mass not yet deposited by precipitation. If the movement is outside to inside, the counter is decremented in like manner. A dedicated computer program applies these statistics, along with an emission inventory and ASTRAP budget statistics, to estimate border fluxes. Such fluxes are normally estimated by season. ASTRAP calculations are compared in Table 1 with the estimates of Galloway et al., which utilize air quality data primarily from 1978.

The negative values in the ASTRAP estimates result from recurvature of trajectories. The two estimates for the Atlantic coastal segments show general agreement, with a maximum in the latitudinal band extending roughly from Washington D. C. to Boston, but the Galloway et al. estimate is about 17% lower and exhibits a steeper gradient for export past the more northern latitudinal bands.

Table 1. Anthropogenic sulfur net mass flux estimates, with meteorological data from 1981.

	Net mass flux (kilotonnes of sulfur)					
	Winter	Spring	Summer	Fall	Annual	GWW*
Atlantic						
25-28 deg N	60	1	-1	12	72	100
28-33 deg N	212	134	76	52	474	410
33-38 deg N	490	428	231	192	1341	860
38-43 deg N	649	559	477	289	1947	1460
43-47 deg N	175	135	98	62	470	930
47-52 deg N	155	13	56	87	311	350
52-57 deg N	101	1	37	175	314	90
57-60 deg N	25	3	-9	154	173	30
Gulf of Mexico	130	-46	-19	133	198	
Mexico	49	7	29	17	102	
Pacific	32	-1	0	22	53	
60° N or Hudson Bay	55	-68	10	66	63	
Emissions	4070	3540	3710	3650	14970	

*Galloway et al. (1984).

References

Galloway, J. N., D. M. Whelpdale, and G. T. Wolff, 1984: The flux of S and N eastward from North America, Atmos. Environ. 18, 2595-2607.

Shannon, J. D., 1979: Computing the long-term, regional-scale net horizontal mass flux of pollutant sulfur, Radiological and Environmental Research Division Annual Report, ANL-79-65, Part IV, Argonne National Laboratory, pp. 44-46.

Shannon, J. D., 1981: A model of regional long-term average sulfur atmospheric pollution, surface removal, and net horizontal flux, Atmos. Environ. 15, 689-701.

SIMULATION OF TRACERS: PARTICLE-IN-CELL MODEL APPLIED FOR CAPTEX AREA

I.-Y. Lee

A particle-in-cell model has been used to make numerical studies of a hypothetical conservative tracer plume over the northeastern United States. The wind fields are generated at five levels by biquadratic approximation from upper air soundings in and near the target area. A σ-coordinate system as shown in Figure 1 is employed. Simulated particles are released at a rate of 60 particles per five minutes from 0900 to 1200 hr EST from an emission point at Dayton, Ohio. The actual initial coördinate of each particle is determined by random selection within a specified volume of air above the emission point. The dimensions of a moving grid are set to be 24 X 24 X 8 units. These grid increments and the time steps for particle transport and diffusion are determined by the plume size in order to obtain adequate spatial resolution, as well as to maintain computational stability.

Subgrid-scale wind fields are generated in the vertical for σ greater than 0.9 by a power law and the first-level wind (σ = 0.9); above, level linear interpolation is used. At present, the assumed values for the power-law exponent are 0.25 during daytime and 0.45 during nighttime. The daytime

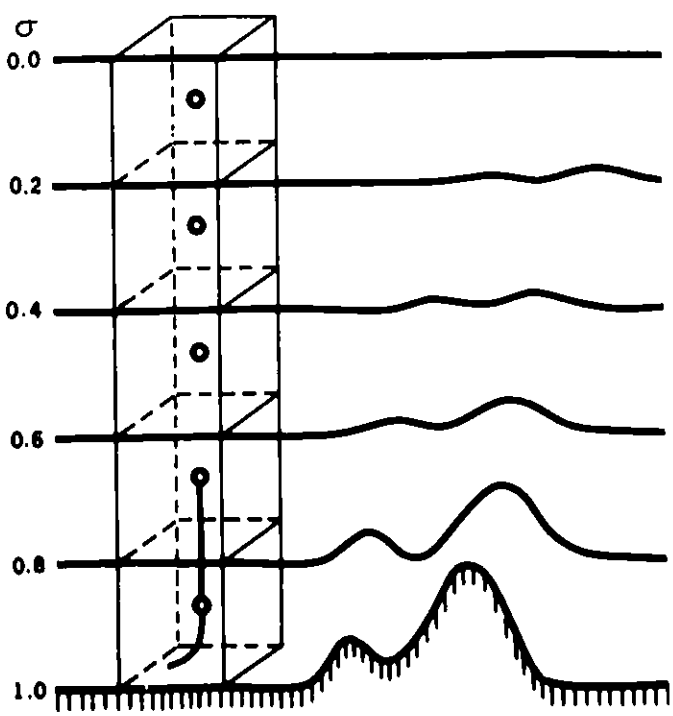

F-g. 1. Model coordinate system.

value of the exponent may need adjustment because it is about twice as large as observations made within 50 m of the surface (Sisterson et al. 1983). Horizontal eddy diffusivities are computed from an empirical formula based upon an analysis by Sheih et al. (1983), and in units of meters squared per second ($m^2\ s^{-1}$) may be written as:

$$D_x = \exp\left[A \ln(\Delta x) - B\right], \tag{1}$$

where Δx denotes the grid size in meters and A = 1.28578 and B = 2.04433 are numerical constants. Vertical eddy diffusivities are formulated by assuming that the values within the planetary boundary layer (PBL) undergo a diurnal variation with maximum at noon, and become insignificant above the PBL. An approximation developed for this purpose is:

$$D_z = D_m \sin\left[\pi(1-\sigma)/\sigma_m\right], \tag{2}$$

where $D_m = 100\sin[\pi(t - t_r)/(t_s - t_r)]$ and $\sigma_m = 0.5\sin[\pi(t - t_r)/(t_s - t_r)]$, and t_r and t_s denote the time of sunrise and sunset, respectively. The cutoff values for D_m and σ_m are set to be 0.05 $m^2\ s^{-1}$ and 10^{-5}, respectively. Results from a test run are presented in Figures 2 and 3. The particle

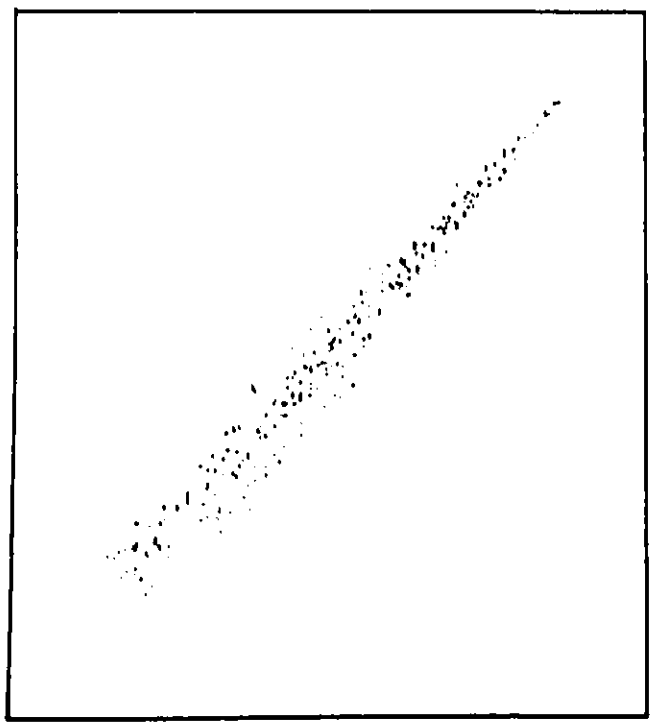

Fig. 2. Particle distribution at 1200 hr EST of day 1.

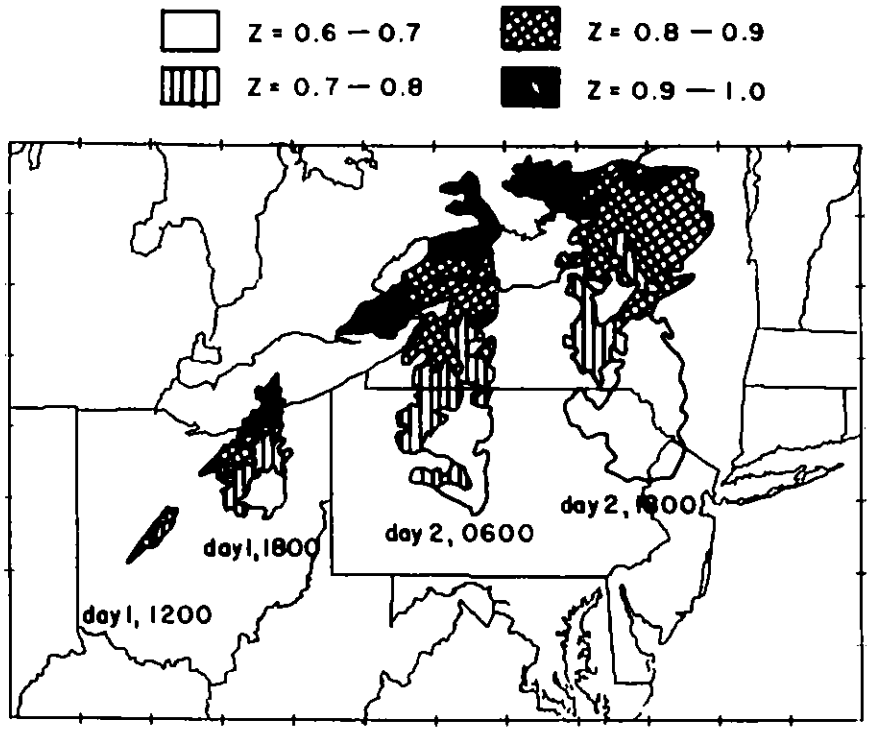

Fig. 3. Plume configurations at 1200 and 1800 hr EST of day 1, and 0600 and 1800 hr EST of day 2 superimposed over a diagrammatic map of the northeastern United States.

distribution at 1200 hr EST (Figure 2), after 3 hr of real time simulation, approximates a Gaussian plume with about 10 deg of dispersion. At 1200 hr EST, simulated particle emissions were terminated; computations were carried out until half of the total particles left the target area. In Figure 3, plume configurations at four different times are presented. Here we see that the initially Gaussian plume structure is highly irregular at 1800 hr EST, mainly because of vertical wind shear, and that the vertical extension of the plume is constrained within about 2000 m from the ground surface ($0.6 < \sigma < 1.0$).

References

Sheih, C. M., P. Frenzen, and R. L. Coulter, 1983: On the measurement of subgrid-scale eddy diffusivity, Preprint Volume, Sixth Symposium on Turbulence and Diffusion, March 22-25, American Meteorological Society, Boston, MA, pp. 253-254.

Sisterson, D. L., B. B. Hicks, R. L. Coulter, and M. L. Wesely, 1983: Difficulties in using power laws for wind energy assessment, Atmos. Environ. 31, 201-204.

A COMPARISON OF ATMOSPHERIC AND NUMERICAL PSEUDODIFFUSIONS

C. M. Sheih and F. L. Ludwig*

It is known that finite-difference approximations for pollutant transport equations introduce artificial numerical diffusion or pseudodiffusion, which could be quite large and might significantly alter the calculated distribution of pollutant concentration. The present study compares the effects of pseudodiffusion reported by many investigators to that of natural diffusion.

Since studies of pseudodiffusion generally report the ratio of peak concentrations of the final and the initial time step of the numerical experiment, it would be desirable to use this ratio as a basis for evaluation. The ratio, here termed an attenuation factor, is denoted by A and B for numerical and atmospheric diffusion, respectively. A relationship between the dispersion coefficient and pollutant concentration can be used to obtain the attenuation factor for atmospheric diffusion. In a two-dimensional isotropic turbulence field, the ratio of the final and initial peak concentrations will be the same as the reciprocal of the ratio of the squares of the corresponding dispersion coefficients, i.e.,

$$\frac{C_{max}(t)}{C_{max}(t_o)} = \frac{\sigma^2(t_o)}{\sigma^2(t)} , \qquad (1)$$

where C_{max} is maximum concentration, σ is the dispersion coefficient, and t is time. The subscript "o" indicates an initial or reference time. Equation (1) indicates that if the dispersion coefficients of the natural dispersion are known, the corresponding attenuation factor of concentration can be estimated. The empirical equation for the horizontal dispersion coefficient given by Gifford (1982) is used and is expressed as:

$$\sigma^2(t) = 2Kt + (V_o/\beta)\,[1 - \exp(-\beta t)]^2$$

$$- (K/\beta)[3 - 4\exp(-\beta t) + \exp(-2\beta t)], \qquad (2)$$

---

*SRI International, 333 Ravenswood Ave., Menlo, CA 94025.

where $K = 5 \times 10^4$ m^2 s^{-1}, $V_o = 0.15$ m^2 s^{-1}, and $\beta = 10^{-4}$ s^{-1}. To compute the horizontal dispersion coefficient from Eq. (2), the travel time t has to be estimated. The travel time depends upon the initial dispersion coefficient, grid size, and advection wind velocity. The initial dispersion coefficient $\sigma(t_o)$ can be estimated by assuming it to be equal to the initial length scale of the pollutant cluster, which is normally given in terms of the grid size in a numerical experiment. However, the grid size and advection wind velocity have to be asssumed according to the ranges of interest for these parameters. In the present study, the advection velocity is assumed to be 10 m s^{-1}, and three grid sizes tested are 0.5, 5, and 50 km. Because the integration times differ from one numerical experiment to another, the relative rather than individual values of A and B are easier to interpret. Therefore, the relative dilution factor $(1 - A)/(1 - B)$ between numerical and atmospheric dilution is shown in the Table 1.

The results corresponding to the 50-km mesh used in regional models appear to be the most significant. The table indicates that there are very few numerical integration schemes that do not have significant problems in numerical diffusion when applied to problems of the regional scale. For the most part, the numerical effects are more than 20% of the natural diffusion for all except the pseudospectral (and related Fourier) methods. There is also qualitative evidence that the importance of the numerical diffusion decreases with increasing elapsed time for a given size. This is not surprising, because all the numerical methods have the most difficulty with sharp gradients. As time proceeds, the gradients are smoothed and the numerical effects are thereby reduced. Thus, while the second-moment method performed well in the tests of Long and Pepper (1976) when applied over an elapsed time of about 3×10^5 s, the same method performed poorly in the tests of Pedersen and Prahm (1974), which for a 50-km grid size represented an elapsed time of only 2.4×10^4 s.

For the grid sizes tested, tne psuedodiffusion of the upstream differencing method always produces larger dispersion than natural diffusion, while the numerical pseudodiffusions for finite element, Crank-Nicolson, pseudospectral, and pseudospectral-associated methods always result in smaller dispersion than natural diffusion. The pseudodiffusion appears to become more important as the grid size increases. For a grid size of 0.5 km used in urban

Table 1. Comparison of Atmospheric dispersion (a) and corresponding numerical dispersion (B) for selected tests of numerical integration methods.

Reference	Numerical Method	A	Dispersion Parameters for Grid Size (km)						Rank
			0.5		5		50		
			B	$\frac{1-A}{1-B}$	B	$\frac{1-A}{1-B}$	B	$\frac{1-A}{1-B}$	
Molenkamp (1968)	Upstream N+1	0.31	0.678	2.14	0.631	1.87	0.917	23	35
	Upstream N	0.40		1.86		1.62		20	34
	Leap Frog	0.86		0.43		0.38		4.7	28
	LAX-Wendroff	0.75		0.78		0.68		8.3	32
	Arakawa Euler	0.86		0.43		0.38		4.7	28
	Arakawa Adams-Bashforth	0.88		0.37		0.33		1.4	20
	Robert Weiss	0.90	0.640	0.27	0.705	0.34	0.957	2.3	26
Orszag (1971)	Arakawa-2nd Order	0.51	0.062	0.52	0.0528	0.52	0.285	0.69	12
	Arakawa-4th order	0.83		0.18		0.18		0.24	7
	Galerkin-Fourier	0.98		0.02		0.02		0.03	1
	Galerkin-Fourier	0.96		0.04		0.04		0.06	4
Anderson & Fattahi (1974)	MacCormack	0.60	0.204	0.50	0.208	0.51	0.680	1.25	19
	Rusanov	0.54		0.58		0.58		1.44	22
	Kotler-Warming Lomax	0.53		0.59		0.59		1.47	24
McRae, et al. (1982)	Fromm	0.55	0.142	0.52	0.159	0.54	0.614	1.17	17
	Crowley	0.73		0.31		0.32		0.70	13
	Finite Element (Chapeau)	0.86		0.16		0.17		0.36	8
	SHASTA	0.51		0.57		0.58		1.27	20

Table 1 (continued)

Reference	Numerical Method	A	Dispersion Parameters for Grid Size (km) 0.5 B	0.5 $\frac{1-A}{1-B}$	5 B	5 $\frac{1-A}{1-B}$	50 B	50 $\frac{1-A}{1-B}$	Rank
Long & Pepper (1976)	Donor Cell, Upwind Difference	0.07	0.110	1.04	0.134	1.07	0.571	2.17	25
	Fully Implicit	0.38		0.70		0.72		1.45	23
	Crank-Nicolson	0.61		0.44		0.45		0.91	14
	Second Moment	0.97		0.03		0.04		0.07	5
	Cubic-Spline	0.91		0.10		0.11		0.21	6
	Galerkin-Chapeau Function	0.98		0.02		0.02		0.05	2
Lee & Meyers (1979)	Fully Implicit, Multi Grid	0.54	0.142	0.54	0.159	0.55	0.614	1.19	18
	Crank-Nicolson, Multi Grid	0.74		0.30		0.83		0.67	11
	Pseudo Spectral	0.98		0.02		0.02		0.05	2
Shannon (1979)	Gaussian Moment Conservation * cos hill, r=4, R=10, $2\pi/240\Delta t$	0.91	0.103	0.10	0.128	0.103	0.560	0.49	9
	Gaussian Moment Conservation * cone r=2, R=5, $2\pi/800\Delta t$	0.41	0.130	0.68	0.0944	0.65	0.389	0.97	16
	Gaussian Moment Conservation * cone r=2, R=5, $2/80\Delta t$	0.43		0.66		0.62		0.93	15
	Gaussian Moment Conservation * cone r=4, R=6, 40, $1.2/40\Delta t$	0.83	0.678	0.53	0.631	0.46	0.917	5.7	31
Pedersen & Prahm (1974)	Mass in Cell	0.46	0.767	2.32	3.725	1.96	0.943	9.5	33
	Second Moment	0.81		0.82		0.69		3.3	27
	Second Moment with width Correction	0.71		1.24		1.05		5.1	29
Christensen & Prahm (1976)	Pseudo Spectral	0.98	0.176	0.02	0.123	0.02	0.443	0.49	10

* r = shape radius in grid units Δx, R = radius of revolution in grid units.

areas, most of the numerical schemes result in smaller dispersion than natural diffusion. However, for the grid size of 50 km frequently used in regional-scale models, about half of the numerical schemes produce larger dispersion than natural dispersion.

References

Anderson, D. and B. Fattahi, 1974: A comparisen of numerical solutions to the advective equation, J. Atmos. Sci. 31, 1500-1506.

Christensen, O. and L. P. Prahm, 1976: A pseudospectral model for dispersion of atmospheric pollutants, J. Appl. Meteorol. 15, 1284-1294.

Gifford, F. A., 1982: Horizontal diffusion in the atmosphere: A Lagrangian-dynamic theory, Atmos. Environ. 16, 505-512.

Lee, H. N. and R. E. Meyers, 1979: On time dependent multi-grid numerical technique, Paper presented at TICOM Meeting, U. of Texas, March 26, 1979.

Long, P. E. and D. W. Pepper, 1976: A comparison of six numerical schemes for calculating the advection of atmospheric pollution, Preprint Volume, Third Symposium on Atmospheric Turbulence Diffusion and Air Quality, Amer. Meteorol. Soc., pp. 181-187.

McRae, G. J., W. R. Goodin, and J. H. Seinfeld, 1982: Numerical solution of the atmospheric diffusion equation for chemically reacting flows, J. Computation Phys. 45, 1-42.

Molenkamp, C. R., 1968: Accuracy of finite-difference methods applied to the advection equation, J. Appl. Meteorol. 7, 160-167.

Orszag, P. E., 1971: Numerical simulation of incompressible flows within simple boundaries: Accuracy, J. Fluid Mech. 49, (Part I), 75-112.

Pedersen, L. B. and L. P. Prahm, 1974: A method for numerical solution of the advection equation, Tellus 26, 594-602.

Shannon, J, D., 1979: A Gaussian moment-conservation diffusion model, J. Appl. Meteorol. 18, 1406-1414.

PARAMETERIZATION OF DRY DEPOSITION OF PARTICULATE SULFUR TO GRASS

M. L. Wesely, D. R. Cook, and R. L. Hart

Eddy-correlation measurements of particulate sulfur dry deposition to a number of surfaces have been obtained during the past several years by Argonne personnel (e.g., Wesely et al. 1983). This article reviews Argonne results from the 1982 Dry Deposition Intercomparison Experiments (DDIE), which took place near Champaign, Illinois, and were coordinated by the Illinois State Water Survey.

As shown in Figure 1, micrometeorological instrumentation was placed over a flat field of mixed grasses. Uniform fetches extended at least 250 m to the south and 400 m to the east and west. Since the eddy-correlation sensors were placed at a height near 6 m, fetch-to-height ratios varied from 40 to 100. Upwind of the grassy field, the terrain was also flat but was covered with crops of soybeans and maize.

The eddy fluxes of momentum, heat, water vapor, and ozone were measured also, with well-practiced techniques. Two flame-photometric detectors (FPD) were used to measure the rapid fluctuations of particulate sulfur. These devices were deployed largely as described by Hicks et al. (1983), except that denuder tubes were used successfully to strip SO_2 from the airstream leading to the FPDs (which otherwise measure total sulfur), and digital analyses eliminated time lags associated with the flow of air from the sampling point to the FPD reaction chamber. Also, one of the FPDs was supplied with SF_6-doped hydrogen for the flame in the burner block, which substantially increased sensitivity and the signal-to-noise ratio (Tanner et al. 1980). Nevertheless, both sensors still produced considerable high-frequency, non-atmospheric noise that increased run-to-run variability (Wesely and Hart 1984).

Results of analysis of approximately 60 half-hour measurement periods are presented in Figure 2. These eddy-correlation flux data were all obtained with the FPD supplied with SF_6-doped hydrogen and provide the least ambiguous data derived from a single sulfur sensor. Analysis of data obtained with the second FPD at the 1982 experiment and with two other configurations of FPDs at

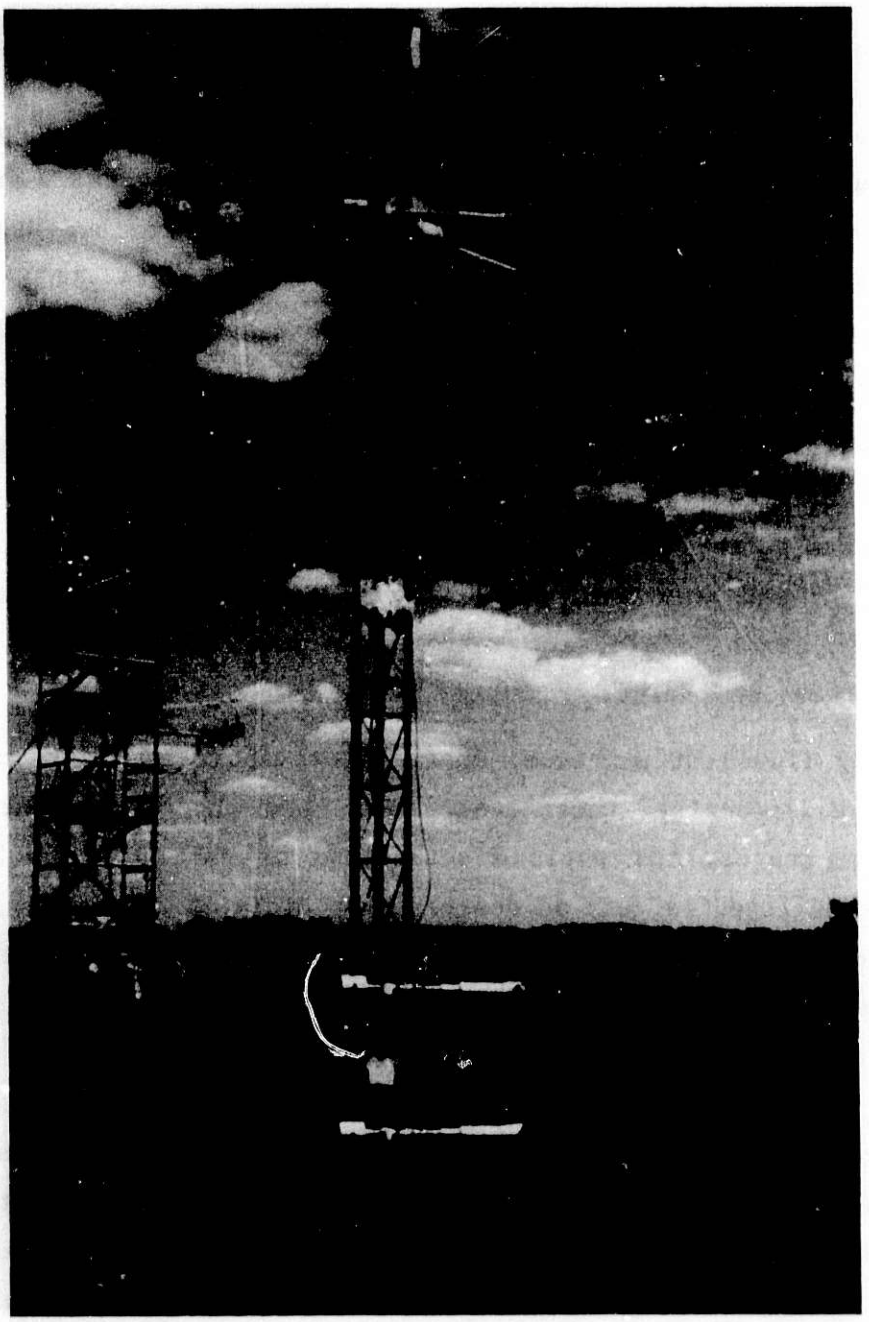

Fig. 1. Photograph of site of the Dry Deposition Intercommparison Experiment. The eddy-correlation sensors extend from a boom from the scaffolding tower in the background, and the equipment to measure mean temperature differences, wind speed, wind direction, and air temperatures is mounted on the triangular tower in the foreground.

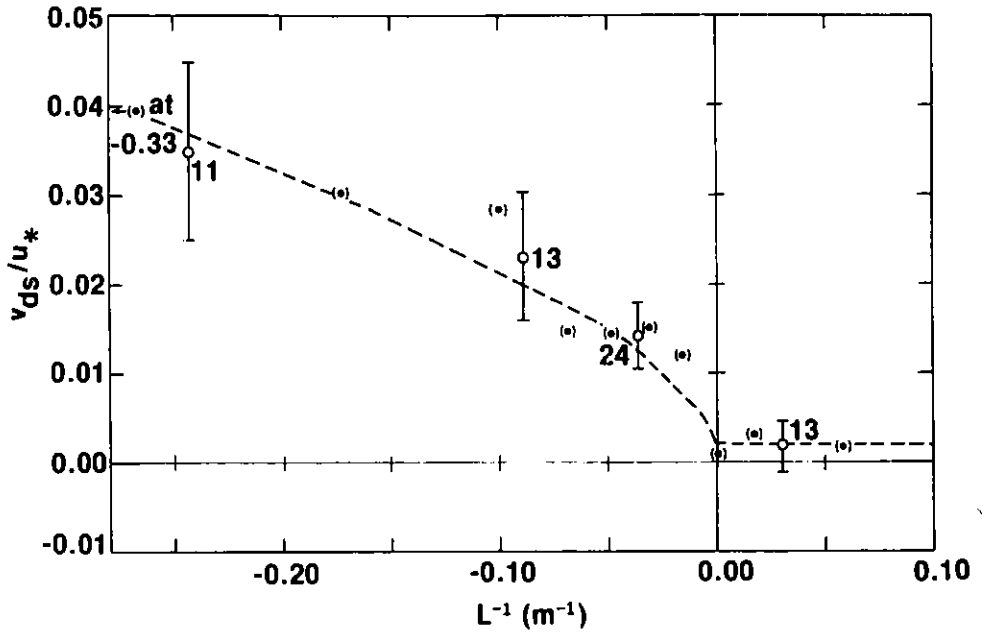

Fig. 2. Normalized surface deposition velocities versus L^{-1} for particulate sulfur. Error bars indicate standard error, and the numbers nearby indicate the number of half-hour samples used in the averages. The dots in parentheses are the same data averaged over alternate intervals of L^{-1}, to help illustrate the relationship of the data to the dashed curve, which represents Eq. (2).

the same site during a pilot experiment in 1981 produced similar results, but with more scatter, most likely a result of lower signal-to-noise ratios.

Figure 2 depicts a micrometeorological approach to parameterization. The surface deposition velocity v_{ds} is calculated from measurements of deposition velocity v_d (the ratio of downward flux density to local mean concentration) at a height near 6 m by subtraction of aerodynamic resistance r_a computed from local micrometeorological parameters such as momentum flux, heat flux, and aerodynamic surface roughness (Wesely and Hicks 1977):

$$v_{ds} = (v_d^{-1} - r_a)^{-1}. \qquad (1)$$

In this way, the effects of variations in r_a are removed and the properties of the surface are isolated as much as possible. The surface deposition velocity, or conductance, is normalized by division by the friction velocity u_* to produce the ordinate in Figure 2. The values of v_{ds}/u_* are plotted

versus the inverse of the Obukhov atmospheric stability parameter L. This deviates from the usual practice of using z/L as the abscissa, where z is the height of measurement, but is justified because values of both v_{ds} and u_* should be independent of height. At this time, it is not clear which, if any, length scale should be used in place of z. One choice is the aerodynamic surface roughness length z_o, but this undoubtedly is not a good indicator of all processes of diffusion and impaction that affect the dry deposition of particulate sulfur.

The dashed curve in Figure 2 is a graphical representation of:

$$v_{ds}/u_* = \begin{cases} 0.002 & L > 0 \\ 0.002[1 + (-300/L)^{2/3}] & L < 0 \ . \end{cases} \qquad (2)$$

For stable and near-neutral conditions when L is small in magnitude or positive, evaluation of Eq. (2) usually leads to values of v_{ds} less than 0.1 cm s^{-1}. Small values are in agreement with wind tunnel results and theoretical predictions (Sehmel 1980; Slinn 1982) for submicron particles where most of the particulate sulfur resides. However, much larger values of v_{ds} (and v_d) are implied by Eq. (2) for unstable conditions when L is strongly negative. The reasons for the large values of measured v_d, which sometimes exceed 0.5 cm^{-1}, are unknown. Perhaps, with the gusty conditions usually found in the afternoon when -L is large, penetration of wind gusts into the plant canopy somehow aids the deposition of fine particles.

The parameterization given by Eq. (2) has been applied to compute deposition velocities averaged over 24-hr periods. For 2-hr periods, mean values of wind speed and vertical temperature differences together with an estimated aerodynamic surface roughness length were utilized in micrometeorological formulae to compute L and u_*. Then v_{ds} was calculated from Eq. (2), and v_d was computed for 2-hr periods via Eq. (1). It was found that the daily average of v_d for 21 days in June during the DDIE varied from 0.05 to 0.21 cm s^{-1}, and produced a grand average of 0.17 cm s^{-1}. By comparison, parameterizations obtained during the 1981 pilot DDIE produced an average v_d of 0.27 cm s^{-1} for 10 days over the grass surface in September. This considerably larger value might be associated with the more windy conditions that occurred in the afternoons during the pilot study.

These results suggest that typical long-term averages of v_d for particulate sulfur at a height near 6 m above moderately tall grass during the summer are near 0.2 cm s^{-1}. This is more than twice the largest values usually suggested for submicron particles in the scientific literature (e.g., Garland 1982). One explanation might be that the eddy flux estimates presented here include the effects of particles larger than 1 μm in diameter, although it is clear that only a very small fraction of such particles are not removed from the sample air by gravitational settling to tubing walls before the FPD is reached. Another consideration is that a gaseous organic sulfate might bias the eddy-correlation results if the substances penetrate through the denuder tubes designed to strip SO_2 from the sample air, have large deposition velocities, and are present at high concentrations during the experiments. The possibility that the latter can occur has been suggested only very recently (Durham et al. 1984).

References

Durham, J. L., L. L. Spiller, D. J. Eatough, and L. D. Hansen, 1984: Dimethyl and methyl hydrogen sulfate in the atmosphere, In: Proceedings, Conference on Environmental Impact of Natural Emissions, Research Triangle Park, NC, Air Pollution Control Association, Pittsburg, PA, (in press).

Garland, J. A., 1982: Field measurements of the dry deposition of small particles to grass, In: Deposition of Atmospheric Pollutants, H.-W. Georgii and J. Pankrath (Eds.), D. Reidel Publishing Co., Dordrecht, Holland, pp. 9-16.

Hicks, B. B., M. L. Wesely, R. L. Coulter, R. L. Hart, J. L. Durham, R. E. Speer, and D. H. Stedman, 1983: An experimental study of sulfur deposition to grassland, In: Precipitation Scavenging, Dry Deposition and Resuspension, Vol. 2, H. R. Pruppacher, R. G. Semonin, and W. G. N. Slinn (Eds.), Elsevier, New York, pp. 933-942.

Sehmel, G. A., 1980: Particle and gas dry deposition: A review, Atmos. Environ. 14, 983-1011.

Slinn, W. G. N. 1982: Predictions for particle deposition to vegetative canopies, Atmos. Environ. 16, 1785-1794.

Tanner, R. L., T. D'Ottavio, R. Garber, and L. Newman, 1980: Determination of ambient aerosol sulfur using a continuous flame photometric detection system. I. Sampling for aerosol sulfate and sulfuric acid, Atmos. Environ. 14, 121-127.

Wesely, M. L. and B. B. Hicks, 1977: Some factors that affect the deposition rates of sulfur dioxide and similar gases on vegetation, J. Air Poll. Contr. Assoc. 27, 1110-1116.

Wesely, M. L., D. R. Cook, R. L. Hart, B. B. Hicks, J. L. Durham, R. E. Speer, D. H. Stedman, and R. J. Tropp, 1983: Eddy-correlation measurements of the dry deposition of particulate sulfur and submicron particles, In: Precipitation Scavenging, Dry Deposition and Resuspension, Vol. 2, H. R. Pruppacher, R. G. Semonin, and W. G. N. Slinn (Eds.), Elsevier, New York, pp. 943-952.

Wesely, M. L. and R. L. Hart, 1984: Variability of eddy-correlation flux measurements due to sensor noise (this report).

VARIABILITY OF EDDY-CORRELATION FLUX MEASUREMENTS DUE TO SENSOR NOISE

M. L. Wesely and R. L. Hart

The eddy-correlation technique has been applied on numerous occasions during the past few years to measure the dry deposition rates of O_3, SO_2, SO_4^{2-}, and NO_x in the atmospheric surface layer. For example, some results on particulate sulfur are discussed elsewhere in this report (Wesely et al. 1984). A consistent difficulty with analysis of these data, especially on sulfur and nitrogen fluxes, appears to be caused by excessive run-to-run variability of the flux estimates. In one study, measured NO_x fluxes changed signs on a few occasions, indicating a surface source of NO_x, and these data points were treated as outliers (Wesely et al. 1982). Such excessive variability could result from a number of environmental factors or procedural inadequacies unique to sulfur and nitrogen substances. We suggest here that a major cause is non-atmospheric signal "noise" generated by the chemical sensors. It appears that the sensors have a relatively poor signal-to-noise ratio for normal ambient atmospheric conditions, and that the sensors are often being operated near their limit of detection. The development of fast-response chemical sensors for eddy correlation is indeed at an early stage compared to development of fast-response temperature, wind, and humidity sensors.

Turbulent transfer processes inherently contain random components, which can usually be described statistically. The effects of signals that contain non-atmospheric noise must be viewed in this context. To illustrate this point, Figure 1 shows the turbulent signals obtained 5.5 m above a grass field during early afternoon. For display purposes, all signals were smoothed with a running mean filter that resulted in severe attenuation of fluctuations at frequencies greater than 1 Hz.

The temperature (T') and humidity (e') fluctuations shown in Figure 1 appear highly correlated, but their correlation with the vertical velocity is less obvious. The time-averaged covariances $\overline{w'T'}$, $\overline{w'e'}$, and $\overline{u'w'}$ are directly proportional to vertical fluxes of sensible heat, latent heat, and momentum. Thus, simple averaging of the appropriate products illustrated in Figure 2 should produce the desired fluxes. For heat, water vapor, and momentum

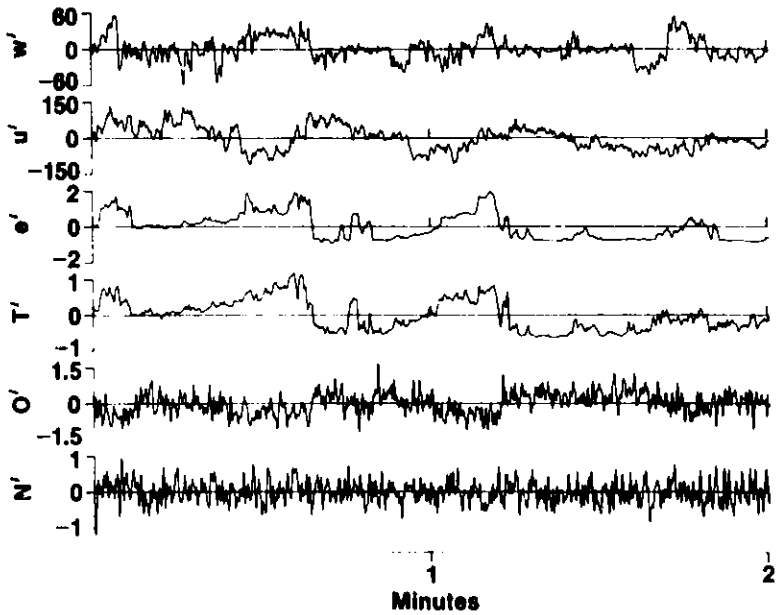

Fig. 1. Turbulent signals for vertical wind speed fluctuations w' (cm s^{-1}), horizontal wind u'(cm s^{-1}), water vapor pressure e' (mb), air temperature T' (C), ozone concentration O' (ppb), and an artificial noise source N' (arbitrary scale) at 5.5 m above grass on 4 June 1983 starting at 1333 hr CST, near Chickasha, Oklahoma.

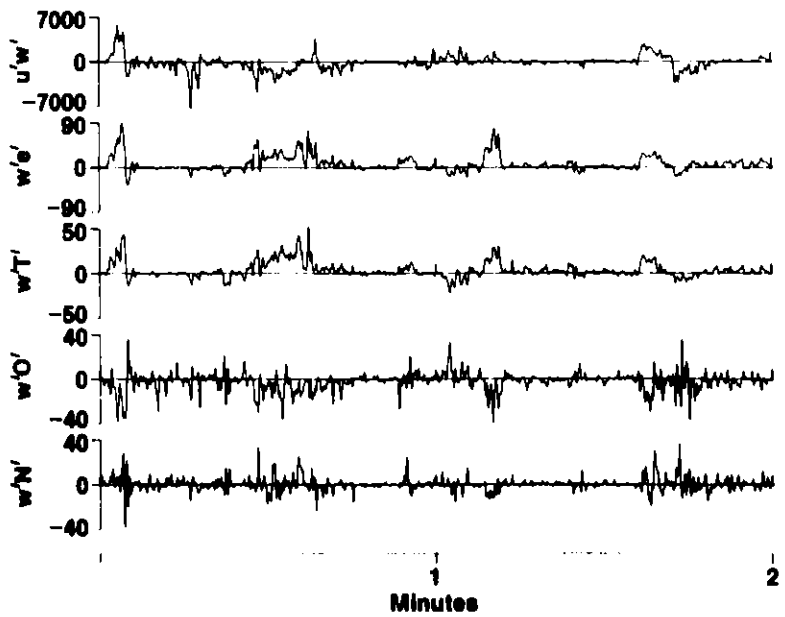

Fig. 2. Products of signals depicted in Figure 1.

fluxes, at least several minutes of averaging are apparently needed. The vertical ozone flux signal w'O', however, is less well behaved and this corresponds to the slight noisiness of the signal for O' shown in Figure 1. From other experiences, it is known that the ozone sensor did not perform as well as it should have; nearly perfect correlation between O' and T' or e' has been found on other occasions with this instrumentation. Because of the ozone sensor noise, longer averaging times are needed to compute a good estimate of $\overline{w'O'}$ than of $\overline{w'T'}$, $\overline{w'e'}$, or $\overline{u'w'}$. Another, extreme case is shown in Figures 1 and 2, namely, the white noise signal N' produced by a computer random number generator. For long averaging times, $\overline{w'N'}$ should be zero, but this is not obvious in Figure 2. Although the noise in both O' and N' is concentrated at high frequencies relative to the flux-carrying eddies, the covariances can still be affected if the amplitude of the noise signal is very large.

An analysis of the effects of bandwith-limited white noise on vertical flux estimates has been carried out. From both a theoretical and empirical standpoint, a reasonable approximation of the likely run-to-run variability due to a random noise source can be expressed as the standard deviation,

$$\sigma_{w'N'} = \sigma_w \sigma_N (f^* T\bar{u}/z)^{-1/2} , \qquad (1)$$

where σ_w and σ_N are the long-term standard deviations for w and N, f^* is an empirical numerical coefficient, T is the total averaging time, $\bar{u}$ is local mean wind speed, and z is the height above the ground. Values of f^* are typically 0.1 for current fast-response humidity sensors (which have very little noise so that a nonzero value usually indicates nonstationary conditions), 0.15 for the O_3 sensor when operating properly (but near 1.5 for the case shown in Figure 2), 0.4 for the sulfur sensor discussed elsewhere in this report (Wesely et al. 1984), and 3 in many cases for typical fast-response NO_x sensors used in the past (Wesely et al. 1982).

The formulation given by Eq. (1) is inexact because the value of f^* depends on the nature and amount of sensor noise in relation to the spectrum of w fluctuations. For sensors that display noise that is almost purely white, however, Eq. (1) should provide a valuable indicator of variability caused only by sensor inadequacies. For example, consider O_3 and NO_x signals

with spectra such as shown in Figure 3. Since excessively large amounts of white noise appear in this type of plot as a line with a slope of +1, particularly at the high frequencies, there is probably a substantial high-frequency white noise component present, and Eq. (1) should produce reasonable approximations. For 13 half-hour runs at the site where the signals for Figure 3 were obtained (Wesely et al. 1982), $\sigma_{w's'}$ = 1.34 ppb cm s^{-1} is computed via Eq. (1), with $f^* = 3$, for NO_x fluxes, and $\sigma_{w's'}$ = 6.28 ppb cm s^{-1} is found for O_3 fluxes when $f^* = 0.4$ is assumed. This agrees well with the standard deviations of 1.40 and 7.33 ppb cm s^{-1} for NO_x and O_3 fluxes, respectively. It should be noted that s represents the total of atmospheric plus artificial noise signals, but that this makes little difference in the comparison just made. If a value of $f^* \approx 0.025$ is chosen, Eq. (1) roughly conforms to the equation given by Wyngaard (1973) for perfect sensors in ideal, stationary, atmospheric conditions. Thus, Eq. (1) provides a smooth extrapolation to the ideal case. Another point is that the actual values of $\sigma_{w's'}$ are larger than those computed via Eq. (1), which should be the case for several hours of real data, during which some degree of large-scale atmospheric nonstationarity and changing surface uptake rates can normally be expected.

The values of f^* used in the previous example were chosen with that particular data set in mind. Thus, Eq. (1) should be used cautiously except

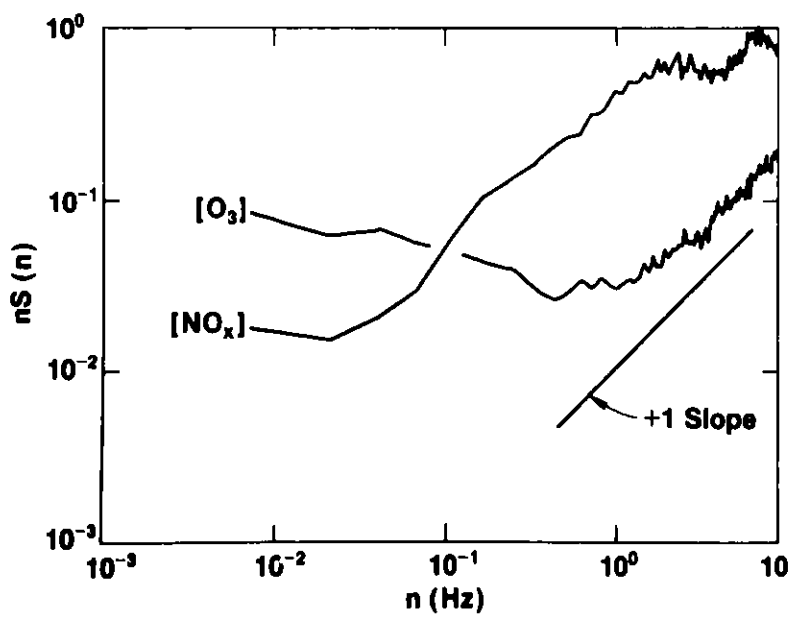

Fig. 3. Spectra of O_3 and NO_x signals obtained for a half-hour period centered at 1515 EST on 16 August 1979 over a soybean field near Lancaster, Pennsylvania, with fast-response chemiluminescent sensors (Wesely et al. 1982). (This vertical axis has an arbitrary scale and is different for each species.)

in the cases where the spectral shape and magnitude of the unwanted signal is very well known in relation to the w signal characteristics. This will occur for many cases of neutral to moderately unstable atmospheric conditions and when the unwanted signal noise is very large in comparison to the expected atmospheric turbulence signals. Both practical experience and Eq. (1) indicate that when relying on the sulfur and nitrogen sensors used in recent years, 5 to 20 times the amount of covariance data must be collected in order to achieve the same confidence of results as obtained with ideal sensors. Hence, further improvement of chemical senors is urgently needed to increase the efficiency of micrometeorological field experiments that utilize eddy correlation to measure and ultimately parameterize pollutant dry deposition.

References

Wesely, M. L, J. A. Eastman, D. H. Stedman, and E. D. Yalvac, 1982: An eddy-correlation measurement of NO_2 flux to vegetation and comparison to O_3 flux, Atmos. Environ. 16, 815-820.

Wesely, M. L., D. R. Cook, and R. L. Hart, 1984: Parameterization of dry deposition of particulate sulfur to grass.

Wyngaard, J. C., 1973: On surface-layer turbulence, In: Workshop on Micrometeorology, D. A. Haugen (Ed.), Amer. Meteorol. Soc., Boston, MA, pp. 101-149.

THE ANL DEPOSITION MONITORING SITE AND ACTIVITIES

D. L. Sisterson, M. L. Wesely, R. L. Hart, and D. R. Cook

Numerical models typically indicate that of the annual delivery of acidifying substances from the atmosphere to the eastern United States about half is by dry processes and the other half is by wet deposition. Wet deposition of pollutants is relatively easy to monitor because precipitation samples can be collected directly by simple procedures. Micrometeorological methods for measuring dry deposition rates of gaseous and particulate pollutant species directly are derived from techniques conventionally used to determine fluxes of sensible heat, moisture, and momentum. These methods, however, currently are too demanding technologically to be acceptable for routine monitoring purposes. An alternative is to measure airborne pollutant concentrations, monitor atmospheric conditions, and observe surface properties, so that parameterizations of deposition velocities can be applied. The average pollutant flux F_c is then obtained as the product of the pollutant concentration $\bar{c}$ and the appropriate deposition velocity v_d. This approach is currently referred to as the "concentration monitoring method."

The deposition monitoring site at Argonne is one of three sites that have been established in the United States to develop and test the concentration monitoring method, as well as other approaches of calculating dry deposition. The Argonne site is taken to be representative of the Midwest; a site operated by the NOAA Atmospheric Turbulence and Diffusion Laboratory and adjacent to the Oak Ridge National Laboratory Walker Branch Research Site is considered representative of the forested Southeast; and the third site, operated by The Pennsylvania State University at the Rock Springs Research Site, is taken to be representative of the hilly Northeast.

The eddy-correlation technique and other micrometeorological methods are used to evaluate and parameterize the deposition velocities of ozone, sulfur dioxide, nitrogen oxides, and particulate sulfur during intensive, short-term, regularly scheduled, intercomparison experiments at all three sites. The results will be interpreted so that deposition velocities can be calculated continuously from routinely obtained meteorological information and applied to air chemistry data to provide long-term (weekly) dry deposition estimates.

Since the diurnal variation of deposition velocities of pollutants can be correlated with their concentrations (most notably ozone), fluxes averaged over several days might not be equal to the product of deposition velocities and concentrations both averaged over the same time period. The evaluation of the inaccuracies that might result from the product of weekly averages, for example, and of methods to reduce those errors constitutes one of the purposes of the three "core" monitoring sites.

In July 1982, an EPA Regional Air Pollution Study (RAPS) building was installed at Argonne's wet deposition site, where weekly and monthly precipitation samples are collected (Sisterson and Wurfel 1980). Routine measurements of precipitation amount are now recorded there with a Belfort* 20.3 cm (8-in) rain gage as well. Since installation of the RAPS building, the site has been extensively cleared of trees and shrubs to improve its use for micrometeorological measurements. This area is now referred to as the "deposition monitoring site", where both wet and dry deposition measurements are being made. Although the site is isolated from local traffic in a remote section of the Argonne grounds, there are many pollution sources within 50 km that are associated with the Chicago metropolitan area to the northeast. A few sources are also located southwest of the site, the largest and closest source being a coal-fired power plant approximately 8 km south-southwest. The Chicago pall and the power plant plume frequently affect otherwise low background pollutant concentrations (Cook and Cobourn 1984).

Routine monitoring of NO and NO_2 (Columbia Scientific Industries* CSI Model 1600 Oxides of Nitrogen Analyzer), O_3 (Dasibi Ozone Monitor Model 1003-AH), and SO_2 (Monitor Laboratories Inc. Model 8850 Sulfur Oxide Analyzer) began in February 1983. Instrumentation calibrations and routine zero and span checks are performed using a Columbia Scientific Industries CSI Model 1800 Programmable Gas Phase Titration Calibrator, which provides built-in remote actuation of the zero and span check points for each air quality instrument. All real-time pollutant concentration sensors sample air through a common 1/2-inch PFA teflon line that leads to a spherical Pyrex glass

*The mention of commercial products in this report does not connote approval or recommendation of these products by Argonne National Laboratory or its sponsors, to the exclusion of other products that may be suitable.

manifold with unassisted flow. The flowrate of the combined instrumentation through the sample line is approximately 3 L min^{-1}. The teflon sample line is approximately 15 m long with the intake at 8.0 m above the ground on a tower adjacent to the RAPS building. The tower and building are shown in Figure 1. Meteorological information on wind speed, wind direction, ambient temperature, and dewpoint temperature are determined at a height of 10 m on another tower approximately 50 m west of the RAPS building.

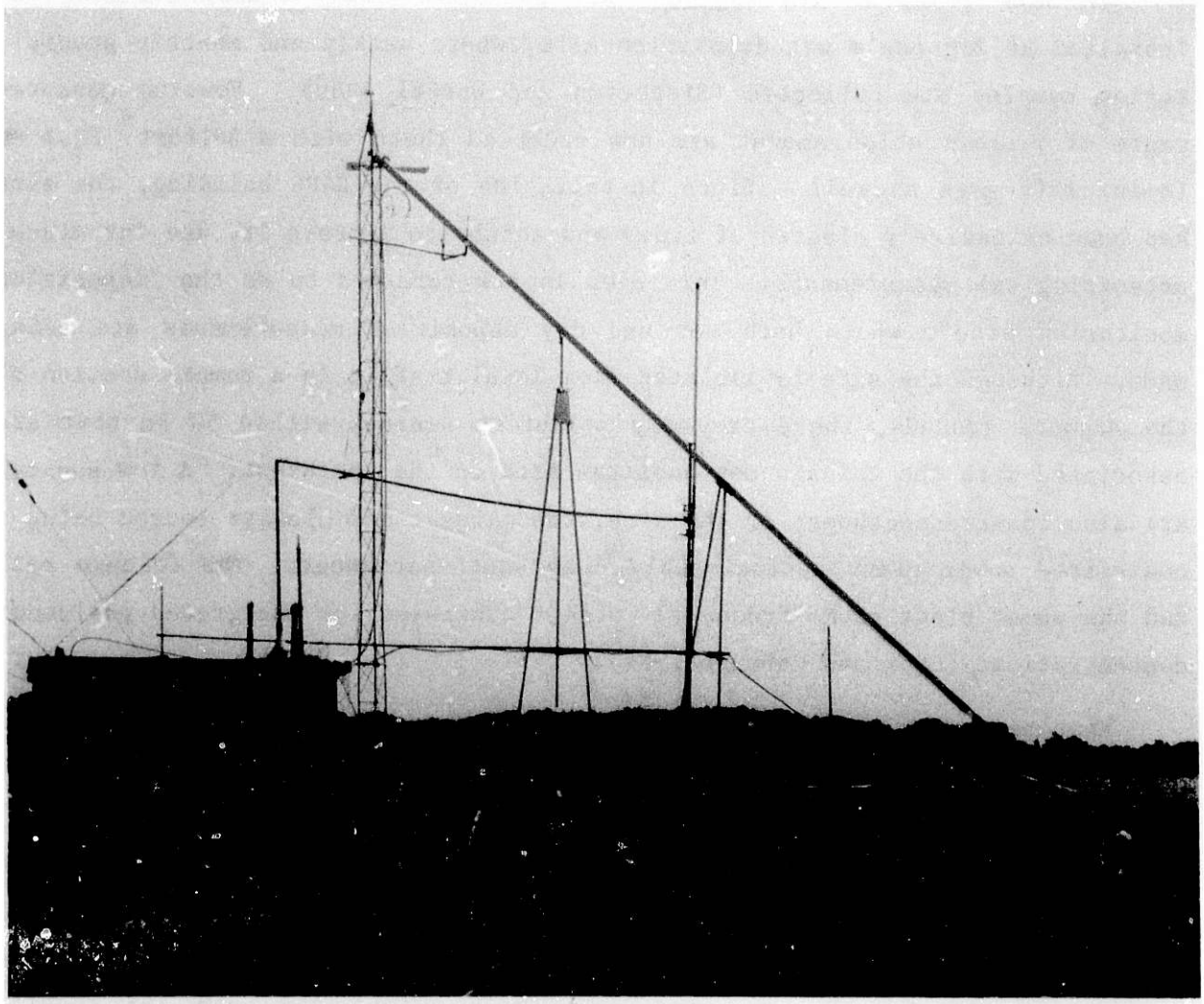

Fig. 1. The ANL deposition monitoring building that houses all air-quality instrumentation and data recording systems. The tram system is the slanting structure between the top of the micrometeorology tower and the surface, and the particle sampling system extends vertically behind and above the center of the tram structure. The sampling heights of 1.0 and 8.5 m are indicated by the shielded aspirators at the center (mounted on a separate mast) of the photo and at the top of the micrometeorology tower, respectively. The air intake for monitored pollutant gases and eddy-correlation measurements is located at 8.0 m on the micrometeorology tower.

As mentioned earlier, the Argonne site also serves as a location to test alternate dry deposition techniques. One candidate technique is the modified Bowen ratio method. To apply this technique, it is necessary to measure mean concentration differences $\Delta\bar{c}$ between two heights. A tram system (shown in Figure 1) carries the intake points of the sample line for SO_2 to heights of 1.0 or 8.5 m, alternately, once every 15 min. Three minutes worth of the 15 min of data is discarded to avoid including data obtained while the tram is in motion and when the sampling systems have not yet equilibrated with conditions at the new position. The lower sampling point is displaced forward so that the more severe deformation of air flow streamlines near the RAPS building can be avoided. A temperature difference ΔT between 1.0 and 8.5 m is measured continuously. The pollutant flux F_c is then calculated as:

$$F_c = H\Delta\bar{c}/(\rho c_p \Delta\bar{T}), \qquad (1)$$

where ρc_p is the heat capacity of the air and H is the sensible heat flux measured by eddy correlation. Since eddy-correlation measurements are not taken at all times, a simple parameterization of $H/(\rho c_p \Delta\bar{T})$ derived partially from eddy-correlation measurements and requiring measurements of the mean wind speed $\bar{u}$ at a 10 m height, $\Delta\bar{T}$, and an estimate of the surface roughness scale length z_o will be applied (e.g., see Wesely et al. 1984). Typically, 30-60 min averages of F_c will be computed. In addition to SO_2, the fluxes of other chemical species will be measured at times with this approach. The species include NO, NO_2, O_3, particulate sulfur by a Meloy Model 285 Sulfur Analyzer equipped with a denuder tube to strip out gaseous sulfur, and particle number concentrations measured with an Thermo-Systems Inc. Model 3030 Electric Aerosol Size Analyzer hooked to a sample line configuration parallel to the tram system, also shown in Figure 1.

Half-hour averages of air quality concentrations and meteorological information are obtained. These data will be used initially to evaluate conditions at the Argonne deposition monitoring site by producing detailed frequency distributions of concentration and meteorological variables similar to those shown by Cook and Cobourn (1983). Also, investigations of the effects of plumes on flux measurements and deposition velocities will be conducted, and methods will be developed for identifying and removing plume influences on daily and weekly concentration averages of the monitored pollutants.

References

Cook, D. R. and W. G. Cobourn, 1984: Some results of recent air-quality measurements (this report).

Sisterson, D. L. and B. Wurfel, 1980: A comparison of the acidity of event and weekly precipitation samples in northern Illinois--a preliminary report, part I, Radiological and Environmental Research Division Annual Report, ANL-80-115, Part IV, Argonne National Laboratory, pp. 68-71.

Wesely, M. L., D. R. Cook, R. L. Hart, and R. E. Speer, 1984: Measurements and parameterization of particulate sulfur dry deposition over grass, J. Geophys. Res. (in press).

SOME RESULTS OF RECENT AIR-QUALITY MEASUREMENTS

D. R. Cook and W. G. Cobourn*

Members of the Atmospheric Physics Program (APP) conducted air-quality and meteorological monitoring near Argonne's Building 181 from 1978 through 1982. Ozone and sulfur dioxide concentrations were measured at a height of 7 m, adjacent to the building, in conjunction with meteorological observations at a nearby tower (Hess 1976). This work proved to be a good training exercise for more extensive air-quality monitoring done later as part of long-term dry deposition monitoring studies. Air-quality monitoring at Building 181 ended in early 1983 when monitoring began at a new site approximately 400 m west of the building (Sisterson et al. 1984).

Ozone and sulfur dioxide data, together with wind direction data obtained from the 45.7-m tower just east of the building, were used to construct quarterly wind direction and pollutant roses. The year of most complete data, 1980, is summarized in Table 1 in terms of daytime (0800 to 2000 CST) and nighttime values. The data collected in 1980 are considered typical of the other years of measurements.

Wind rose data for 1980 show that SW winds occur 31% of the time on an annual average, with NW (28%) and NE (26%) being slightly less frequent. During the months of April to September, SW winds occur 33% of the time, with NE (27%) being the next most frequent. Southwest winds are particularly common (40%) during June-August. Northwest winds are most common (35%) during October-March, with SW (27%) being second most common.

Table 1 shows that local pollution sources significantly influence SO_2 concentrations measured at Argonne. The moderately large (nominally 1100 MW) Lockport power plant and a large refinery are 10 and 8 km, respectively, southwest of Argonne. These facilities lie in a river valley about 50 m lower in elevation than Building 181, with the height of the power plant stacks

*Faculty Research Participant, Division of Educational Programs, from the University of Louisville, KY.

Table 1. Quarterly and annual average O_3 and SO_2 concentrations (ppb) from all wind directions combined, plus the largest and smallest quarterly average O_3 and SO_2 concentrations (ppb) with accompanying wind direction. These are listed as a function of time of day: D - day, N - night, T - day plus night. When concentrations from two directions are large, both are listed.

Pollutant	Quarter 1980														
	1			2			3			4			Annual		
	D	N	T	D	N	T	D	N	T	D	N	T	D	N	T
O_3, all dir.:	23	15	19	40	17	29	43	18	30	14	6	10	30	14	22
SO_2, all dir.:	15	11	13	15	15	15	27	23	25	~17	~14	~15	~19	~16	~17
O_3, largest:	30 NSW	18 SSW		54 SSW 53 SW	27 SSW		50 WSW 49 SSW	28 SSW 26 SW		18 WSW 17 NW	10 NW 8 SSW				
O_3, smallest:	15 ESE 15 ENE	8 SE 7 ESE		22 NE	10 ESE		35 NNE 33 NE	8 NNW 7 SE		7 ESE 5 NE	4 ESE 3 NE				
SO_2, largest:	33 SW 32 ESE	27 SW 18 ENE		30 SW 24 ENE	23 SW 22 ESE		39 SW 34 SSE	28 NE 27 NNW		No data					
SO_2, smallest:	6 NNW 6 NW	6 NW 5 WNW		7 NNE 7 NNW	8 NW		20 NNE 20 SE	18 NW 16 NNE		No data					

ranging from 106 to 152 m. This elevation difference, in conjunction with common SW winds, sometimes cause Building 181 to be subjected to pollutant concentrations several times larger than the maxima from other directions. This is especially true during the summer, when sulfur emissions tend to be greatest as a result of high electrical demand for air conditioning. Occasional NE and E winds during the summer months sometimes result in large amounts of pollutants being transported to Argonne from the steel mills and refineries around the southern rim of Lake Michigan, or from the Ridgeland power plant (700 MW) to the NE. The wind directions (NW-NNE) that result in the lowest measured SO_2 concentrations at Argonne are least frequent during the summer months, when the emissions of the power plants are usually greatest, and most frequent in the winter, when emissions are usually less.

Seasonal and diurnal variations of O_3 concentration occur, irrespective of wind direction. Times of greater solar irradiation (daytime, summer), and therefore greater photochemical activity, result in higher O_3 concentration, as opposed to the lower concentrations that occur during times of less or no solar irradiation (winter, nighttime). A slight diurnal variation in SO_2 concentration is detectable, but this variation is much less pronounced than for O_3. This slight variation is a result of the general difference in atmospheric stability between day and night, plus perhaps local removal of O_3 by chemical reaction with NO emitted in the vicinity.

The O_3 concentration measured at Argonne is affected more by air mass age and proximity to the large Chicago urban area than by local sources. The only exception occurs when a plume from the Lockport power plant passes over Argonne so that the NO in the plume reacts with O_3, thereby reducing O_3 concentration significantly. The largest O_3 concentrations are measured for generally SW winds, the direction most common on the backside of high-pressure areas. Typically, the photochemistry that produces O_3 has had a long time to occur in this situation, resulting in higher O_3 concentrations. Somewhat lower O_3 concentrations are measured with NNW-SE winds, a result partially of reaction with urban NO sources to the NE-SE, but also because lower O_3 concentrations occur in newer, cleaner air masses, which often attend NW-NE wind directions.

In summary, the proximity of Argonne to Chicago and to fossil-fuel power plants and refineries results in frequent and often significant intrusions of

high pollutant concentrations over the present air-quality monitoring station. However, background-level concentrations (unaffected by local or nearby urban sources), though occuring from limited directions and with lesser frequency, can be measured and will provide valuable information for determining the impact of local and urban sources on the air-quality measured at the monitoring station. This information can be used to adjust parameterizations of pollutant dry deposition, thus yielding results more representative of a less urbanized area.

References

Hess, P. E., 1976: Processing Argonne weather data, Radiological and Environmental Research Division Annual Report, ANL-76-88, Part IV, Argonne National Laboratory, pp. 140-152.

Sisterson, D. L., M. L. Wesely, R. L. Hart, and D. R. Cook, 1984: The ANL deposition monitoring site and activities (this report).

MONTHLY METEOROLOGICAL DATA SUMMARIES AT ANL

R. L. Hart

Routine monthly processing of meteorological data has been resumed by personnel of the Atmospheric Physics Program in support of studies to develop and test techniques to measure dry deposition of acidifying substances at the deposition monitoring site near Building 181 (Sisterson et al. 1984). The old data-acquisition system (Hart and Haumann 1975) was damaged by lightning and had not been operating properly since October of 1981. A new, microprocessor-controlled data logger (a Campbell Scientific Model CR7 Measurement and Control System*) has been installed to replace the old system. The new system employs the same set of sensors that were previously used, except that diffuse solar radiation is no longer being measured, and all air quality monitoring has been transferred to the deposition monitoring site. The CR7 was installed in July 1983 using the amplifiers from the old system. Subsequently, the resistance bridges and associated amplifiers from the old system were discarded and replaced with constant-current power supplies. All inputs to the present system are either voltages or pulses, the latter being for the cup anemometers.

The CR7 not only performs real-time conversion of inputs into standard units, but also averages data over user-defined time intervals, detects minima and maxima, converts dewpoint temperatures into vapor pressures, computes standard deviations, and averages winds vectorally. Results are printed out as well as recorded on cassette magnetic tape for additional computer analysis. Once each month the taped data are processed on an DEC LSI-11/73 minicomputer to produce monthly summaries.

Data are summarized in tabular form, similar to previous data displays (Hess 1976). A daily summary, as shown in Table 1, tabulates hourly averages of ambient and dewpoint temperatures at a height of 1.5 m, temperature

---

*The mention of commerical products in this report does not connote approval or recommendation of these products by Argonne National Laboratory or its sponsors, to the exclusion of other products that may be suitable.

Table 1. Sample of a typical daily summary.

ARGONNE NATIONAL LABORATORY

17 MAR 84

HR	AMB. TEMP. CELCIUS	DEW POINT CELCIUS	DT DZ C/M	VAPOR PRES. MB	REL. HUM. %	WIND SPEED 1.5M METERS/SECOND	WIND SPEED 6.0M METERS/SECOND	WIND SPEED 44.5M METERS/SECOND	DIR. 44.5M DEG	SIGMA DIR. DEG	RADIATION SOLAR W/M**2	RADIATION NET W/M**2	SOIL TEMP. 10CM DEGREES CELCIUS	SOIL TEMP. 100CM DEGREES CELCIUS	SOIL TEMP. 305CM DEGREES CELCIUS
1	-0.9	-3.3	0.002	4.63	82.	2.8	4.1	6.5	80.	8.4	0.	-7.	-0.1	3.2	8.0
2	-1.0	-3.0	-0.001	4.75	84.	3.2	4.8	6.7	76.	10.3	0.	-6.	-0.1	3.2	8.0
3	-1.3	-3.1	-0.002	4.74	86.	3.3	4.1	7.0	78.	9.1	0.	-6.	-0.1	3.2	8.0
4	-1.3	-3.0	-0.001	4.75	87.	2.5	4.4	6.1	77.	9.9	0.	-6.	-0.1	3.2	8.0
5	-1.4	-3.0	-0.004	4.78	88.	2.1	4.2	5.7	79.	10.3	0.	-6.	-0.1	3.2	8.0
6	-1.9	-3.2	-0.008	4.70	90.	3.6	5.4	7.6	74.	9.9	0.	-6.	-0.1	3.2	8.0
7	-2.4	-3.3	-0.006	4.64	93.	2.7	3.2	6.6	77.	10.6	4.	-3.	-0.1	3.2	8.0
8	-2.3	-3.5	-0.008	4.56	91.	1.2	3.6	4.9	81.	10.9	15.	3.	-0.1	3.2	8.0
9	-2.3	-3.9	-0.016	4.43	88.	3.2	5.0	7.1	70.	8.4	42.	21.	-0.1	3.2	8.0
10	-2.0	-4.0	-0.020	4.39	85.	4.0	5.0	8.7	73.	9.9	71.	39.	-0.1	3.2	8.0
11	-2.3	-4.4	-0.026	4.22	83.	4.3	6.7	9.9	68.	9.2	103.	62.	-0.1	3.2	8.0
12	-2.5	-4.7	-0.036	4.14	83.	4.7	6.8	10.0	65.	10.0	168.	108.	-0.1	3.2	8.0
13	-2.6	-4.5	-0.021	4.21	86.	3.2	5.3	7.3	77.	10.1	104.	65.	-0.1	3.2	8.0
14	-2.4	-4.9	-0.025	4.08	81.	3.1	4.7	6.7	76.	9.7	100.	59.	-0.1	3.2	8.0
15	-2.5	-4.8	-0.021	4.10	83.	2.8	4.2	6.3	73.	9.3	60.	30.	-0.1	3.2	8.0
16	-2.7	-4.3	-0.019	4.26	87.	0.8	2.5	3.9	67.	11.2	22.	7.	-0.1	3.2	8.0
17	-2.8	-3.7	-0.016	4.48	93.	0.2	2.3	4.4	58.	8.7	19.	4.	-0.1	3.2	8.0
18	-2.6	-3.2	-0.005	4.71	96.	0.6	2.6	4.5	63.	9.7	17.	1.	-0.1	3.2	8.0
19	-2.4	-3.0	0.000	4.76	95.	0.0	1.9	3.7	65.	8.4	0.	-3.	-0.1	3.2	8.0
20	-2.3	-2.8	0.007	4.87	96.	0.0	1.6	3.2	67.	8.5	0.	-5.	-0.1	3.2	8.0
21	-2.1	-2.7	0.016	4.90	96.	0.0	2.2	4.0	68.	9.1	0.	-6.	-0.1	3.2	8.0
22	-2.3	-3.2	0.011	4.68	92.	0.0	2.2	4.0	75.	8.8	0.	-6.	-0.1	3.2	8.0
23	-2.3	-3.6	0.005	4.55	90.	0.0	2.3	4.1	71.	8.8	0.	-6.	-0.1	3.2	8.0
24	-2.4	-3.7	0.006	4.50	90.	0.0	1.6	3.1	75.	10.1	0.	-5.	0.0	3.2	8.0
MEAN	-2.1	-3.6	-0.008	4.53	88.	2.0	3.8	5.9		9.6	30.	14.	-0.1	3.2	8.0
VECTOR WIND								5.8	73.						
MAX	-0.8	-2.5						16.1			234.	156.	0.1		
TIME	0009	2027						1144			1120	1120	1419		
MIN	-3.0	-5.3						0.6				-7.	-0.1		
TIME	1632	1348						1555				0014	2004		

Table 2. Sample of a typical monthly summary by hour.

ARGONNE NATIONAL LABORATORY

MAR 84

HR	AMB. TEMP. CELCIUS	DEW POINT CELCIUS	DT DZ C/M	VAPOR PRES. MB	REL. HUM. %	WIND SPEED 1.5M METERS/SECOND	WIND SPEED 6.0M METERS/SECOND	WIND SPEED 44.5M METERS/SECOND	DIR. 44.5M DEG	SIGMA DIR. DEG	RADIATION SOLAR W/M**2	RADIATION NET W/M**2	SOIL TEMP. 10CM DEGREES CELCIUS	SOIL TEMP. 100CM DEGREES CELCIUS	SOIL TEMP. 305CM DEGREES CELCIUS
1	-3.1	-5.5	Ø.ØØ91	4.14	82.	Ø.8	2.3	4.7	13.	11.Ø	Ø.	-22.	Ø.6	3.4	8.Ø
2	-3.2	-5.4	Ø.ØØ95	4.19	85.	Ø.9	2.2	4.7	14.	8.4	Ø.	-22.	Ø.5	3.4	8.Ø
3	-3.4	-5.4	Ø.1Ø4	4.2Ø	86.	Ø.9	2.1	4.8	16.	8.5	Ø.	-22.	Ø.5	3.4	8.Ø
4	-3.6	-5.5	Ø.1Ø1	4.18	87.	Ø.9	2.2	4.9	8.	8.7	Ø.	-22.	Ø.5	3.4	8.Ø
5	-3.8	-5.8	Ø.ØØ99	4.13	86.	1.1	2.5	5.Ø	3.	8.3	Ø.	-22.	Ø.5	3.4	8.Ø
6	-4.Ø	-6.Ø	Ø.ØØ97	4.Ø5	86.	1.1	2.5	4.9	1Ø.	8.Ø	1.	-21.	Ø.5	3.4	8.Ø
7	-3.7	-5.6	Ø.ØØ77	4.19	87.	1.1	2.7	4.8	14.	1Ø.6	31.	-9.	Ø.4	3.4	8.Ø
8	-2.6	-4.9	Ø.ØØØ6	4.4Ø	85.	1.4	3.2	4.8	19.	1Ø.9	119.	23.	Ø.4	3.4	8.Ø
9	-1.6	-4.8	-Ø.Ø16	4.4Ø	79.	1.8	3.5	4.8	28.	12.5	225.	67.	Ø.4	3.4	7.9
1Ø	-Ø.7	-4.8	-Ø.ØØ37	4.41	74.	1.8	3.7	5.1	3Ø.	12.5	345.	121.	Ø.4	3.4	7.9
11	Ø.Ø	-5.1	-Ø.ØØ51	4.35	69.	2.1	3.8	5.3	27.	15.3	411.	152.	Ø.5	3.4	7.9
12	Ø.4	-5.4	-Ø.ØØ58	4.26	66.	2.2	4.Ø	5.4	27.	14.7	4Ø6.	161.	Ø.5	3.4	7.9
13	Ø.7	-5.Ø	-Ø.ØØ6Ø	4.35	66.	2.Ø	3.7	5.2	24.	15.7	381.	151.	Ø.6	3.4	7.9
14	1.Ø	-5.1	-Ø.ØØ55	4.35	65.	2.1	3.8	5.3	3Ø.	16.3	351.	137.	Ø.7	3.4	7.9
15	1.Ø	-5.1	-Ø.ØØ47	4.34	65.	2.2	3.9	5.4	28.	18.5	3Ø1.	111.	Ø.8	3.4	7.9
16	Ø.8	-5.3	-Ø.ØØ22	4.27	66.	1.9	3.5	5.3	24.	18.9	197.	63.	Ø.8	3.4	7.9
17	Ø.5	-5.3	-Ø.ØØØ5	4.27	67.	1.4	3.Ø	5.1	26.	13.5	113.	24.	Ø.9	3.4	7.9
18	-Ø.3	-5.8	Ø.ØØ21	4.17	68.	1.2	2.7	5.Ø	39.	19.Ø	3Ø.	-14.	Ø.9	3.4	7.9
19	-1.Ø	-5.7	Ø.ØØ5Ø	4.18	72.	1.1	2.5	4.9	37.	9.2	Ø.	-22.	Ø.8	3.4	7.9
2Ø	-1.6	-5.6	Ø.ØØ71	4.17	75.	1.1	2.5	4.8	38.	1Ø.Ø	Ø.	-23.	Ø.8	3.4	7.9
21	-2.Ø	-5.6	Ø.ØØ96	4.14	77.	Ø.9	2.3	4.9	4Ø.	8.3	Ø.	-22.	Ø.8	3.4	7.9
22	-2.3	-5.5	Ø.ØØ96	4.17	78.	Ø.8	2.4	4.8	42.	9.7	Ø.	-23.	Ø.7	3.4	7.9
23	-2.4	-5.3	Ø.ØØ83	4.21	8Ø.	1.8	2.4	4.8	33.	8.7	Ø.	-22.	Ø.7	3.4	7.9
24	-2.8	-5.5	Ø.ØØ7Ø	3.96	78.	Ø.9	2.4	4.4	18.	8.8	Ø.	-23.	Ø.6	3.3	7.7

Table 3. Sample of a typical monthly summary by day.

ARGONNE NATIONAL LABORATORY

MAR 84

DAY	AMB. TEMP.	DEW POINT	WIND SPEED 1.5M	6.ØM	44.5M	VECTOR-WIND SPEED	DIR.	SIGMA DIR.	RADIATION SOLAR	NET	SOIL TEMP. 1ØCM	1ØØCM	3Ø5CM
	CELCIUS		METERS/SECOND				DEG		W/M**2		DEGREES CELCIUS		
1	-4.Ø	-1Ø.2	Ø.2	Ø.5	3.2	2.2	271.	11.8	166.	13.	Ø.4	4.1	8.3
2	-3.7	-1Ø.4	Ø.3	Ø.Ø	3.1	2.3	15.	17.8	2Ø3.	1Ø.	Ø.4	4.Ø	8.2
3	-4.4	-9.4	Ø.1	Ø.2	2.7	2.1	18Ø.	13.5	2Ø6.	12.	Ø.4	3.9	8.2
4	-3.1	-6.Ø	Ø.8	2.3	4.8	4.3	1Ø7.	9.2	32.	1.	Ø.3	3.8	8.3
5	-1.7	-3.8	2.5	4.8	7.3	7.Ø	264.	7.7	55.	4.	Ø.2	3.8	8.2
6	-5.6	-7.8	Ø.7	2.3	3.7	2.5	322.	12.6	93.	11.	Ø.2	3.7	8.2
7	-8.2	-1Ø.9	Ø.8	2.1	4.2	3.1	1Ø1.	11.3	148.	16.	Ø.2	3.6	8.2
8	-7.8	-11.Ø	2.2	3.9	6.5	5.4	23.	9.3	14Ø.	12.	Ø.1	3.6	8.1
9	-9.8	-12.2	Ø.7	1.9	4.1	3.5	267.	9.2	147.	Ø.	Ø.1	3.5	8.1
1Ø	-8.Ø	-1Ø.3	2.4	4.Ø	6.5	5.9	249.	9.Ø	2Ø9.	2Ø.	Ø.Ø	3.5	8.1
11	-8.7	-17.5	2.1	3.4	4.9	3.9	314.	16.5	235.	19.	Ø.Ø	3.4	8.1
12	-7.6	-11.3	1.Ø	2.6	4.5	4.1	1ØØ.	1Ø.9	81.	16.	-Ø.1	3.4	8.1
13	-1.8	-4.Ø	Ø.1	1.3	2.2	2.Ø	6Ø.	14.4	1Ø1.	24.	-Ø.1	3.4	8.1
14	-Ø.4	-1.8	1.2	2.5	4.1	4.Ø	146.	1Ø.3	87.	22.	-Ø.1	3.3	8.Ø
15	4.9	3.8	1.1	2.9	5.7	1.5	143.	17.1	34.	25.	-Ø.1	3.3	8.Ø
16	-2.Ø	-4.4	2.1	5.3	7.7	7.1	22.	1Ø.7	7Ø.	4Ø.	-Ø.1	3.3	8.Ø
17	-2.1	-3.6	2.Ø	3.8	5.9	5.8	73.	9.6	3Ø.	14.	-Ø.1	3.2	8.Ø
18	-1.6	-4.1	1.Ø	2.8	4.4	4.2	39.	8.8	81.	15.	Ø.Ø	3.2	7.9
19	-Ø.6	-1.6	1.1	3.1	5.2	5.1	66.	1Ø.1	3Ø.	8.	Ø.Ø	3.2	7.9
2Ø	1.4	Ø.3	1.9	2.7	5.1	3.Ø	183.	11.2	51.	28.	Ø.Ø	3.2	7.9
21	Ø.4	Ø.Ø	Ø.7	2.5	5.3	4.7	282.	9.5	25.	2Ø.	Ø.Ø	3.2	7.8
22	Ø.8	-2.4	2.6	4.3	6.2	6.Ø	3Ø1.	1Ø.5	57.	2.	Ø.Ø	3.1	7.8
23	1.7	-5.6	Ø.1	1.4	3.3	1.5	317.	22.4	258.	8Ø.	Ø.2	3.Ø	7.8
24	2.5	-3.9	1.2	2.2	4.5	3.6	96.	1Ø.4	126.	57.	Ø.6	3.Ø	7.7
25	2.7	-3.Ø	2.1	3.9	6.3	6.1	45.	8.8	73.	28.	1.1	3.Ø	7.7
26	3.3	-2.5	1.9	2.4	4.3	4.1	74.	1Ø.4	216.	1Ø1.	1.8	3.Ø	7.7
27	2.6	Ø.6	2.Ø	2.6	6.1	5.9	55.	8.2	68.	45.	2.6	3.1	7.6
28	3.3	-2.6	4.2	6.4	9.Ø	8.8	25.	9.1	2Ø5.	88.	2.9	3.2	7.6
29	2.5	-3.7	2.2	3.9	6.Ø	5.8	4.	12.8	185.	75.	2.6	3.3	7.5
3Ø	2.7	-3.8	Ø.8	2.5	4.2	4.1	324.	1Ø.9	137.	52.	2.7	3.4	7.5
31	2.7	-5.2	Ø.4	1.4	3.2	1.Ø	359.	23.5	257.	1Ø5.	3.2	3.5	7.5
MEAN	-1.6	-5.4	1.4	2.8	5.Ø	1.5	24.	12.5	123.	31.	Ø.6	3.4	7.9

difference between 1.5 and 6.0 m, water vapor pressure and relative humidity at 1.5 m, wind speeds at 1.5, 6.0, and 44.5 m, wind direction and the standard deviation of the wind direction at 44.5 m, solar and net radiation, and soil temperature at -10 cm, -100 cm, and -305 cm. Daily averages for all of the above and vector-averaged wind speed and direction at 44.5 m are given. Also listed are the daily maxima and minima of ambient and dewpoint temperatures, 44.5 m wind speed, -10 cm soil temperature, and net radiation. These maxima, plus that for solar radiation, are presented along with the time of each occurrence.

Two monthly summaries are tabulated. An example of averages by hour of the data is given in Table 2. This provides the average diurnal cycle of each meteorological variable for the month. The wind directions are vector averaged. The second monthly summary, illustrated in Table 3, provides daily averages of ambient and dewpoint temperatures, wind speeds at 1.5, 6.0, and 44.5 m, vector-averaged wind speed and direction and standard deviation of wind directon at 44.5 m, solar and net radiation, and soil temperatures at all three levels. Trends during the month can be seen from this summary.

References

Hart, R. L. and J. R. Haumann, 1975: An improved meteorological data acquisition system, Radiological and Environmental Research Division Annual Report, ANL-75-3, Part IV, Argonne National Laboratory, pp.142-150.

Hess, P. E., 1976: Processing Argonne weather station data, Radiological and Environmental Research Division Annual Report, Argonne National Laboratory ANL-76-88, Part IV, pp. 140-152.

Sisterson, D. L., M. L. Wesely, R. L. Hart, and D. R. Cook, 1984: The ANL deposition monitoring site and activities (this report).

LOCAL EFFECTS OF WINTER SNOW COVER ON SPRING SOIL AND AIR TEMPERATURES

D. R. Cook

Statistical relationships between snow cover and soil and air temperatures during winter months have been studied often; however, few studies have investigated relationships between snow cover and temperatures measured sometime later. In one case, a study by Foster et al. (1982), winter air temperature at the geographic center of the Eurasian continent was found to be correlated with the extent of autumn snow cover over the continent. It was concluded that autumn snow cover extent affects the strength of the winter Asiatic anticyclone, and thereby the temperatures associated with it.

In the present study, statistical relationships between winter snow cover and spring soil and air temperatures are examined. It is likely that any significant relationships found in such studies are at least partially a consequence of synoptic and regional-scale weather factors. These factors may, in turn, be affected by snow-cover-related changes in the surface energy budget. National Weather Service data on snow at Midway Airport are used in conjunction with soil and air temperature measurements made during 1950-1981 at a single small area at Argonne National Laboratory (Moses and Bogner 1967; Hess 1976), to determine coefficients of correlation and levels of significance for snow parameters versus temperatures. The parameters from Argonne are annual and spring monthly (March, April, May, June) averaged air and soil temperatures (measured at 5.5 m above the surface and 10, 100 and 305 cm below the grass surface, respectively) and the Julian date at which 10° C was reached at each of the soil depths. The parameters from Midway Airport are (a) the latest Julian date for which one inch of snow cover was reported at the end of the winter, (b) the total number of days in the winter when one inch or more snow depth was recorded at 0600 CST, and (c) the longest continuous duration of snow cover of one inch or more during the winter.

Some of the statistics computed for these data are summarized in Table 1. Only correlations with significance of 90% or greater are shown. With the exception of latest Julian date, correlations between snow cover and monthly soil temperature are greatest for May. It might be expected that the correlations would be greatest for April, but the apparent effect of snow

Table 1. Coefficients of correlation (r) and levels of significance (s, in %) for Midway Airport snow cover parameters versus Argonne National Laboratory soil temperature parameters.

		Soil Temperature Parameters												
Snow Cover	Statistics	10° C Date	Annual			March	April			May			June	
Parameters		100 cm	10 cm	100 cm	305 cm	305 cm	10 cm	100 cm	305 cm	10 cm	100 cm	305 cm	100 cm	305 cm
Latest Date of one inch snow cover	r							-0.35						
	s							92						
Total days of snow cover	r	-0.38	0.50	0.39	0.40					0.51	0.38	0.41		0.42
	s	94	99	94	95					99	94	96		97
Longest duration of snow cover	r	-0.42	0.50	0.41	0.35	0.35	0.38	0.43	0.37	0.45	0.44	0.45	0.34	0.36
	s	97	99	96	91	92	95	97	94	98	98	98	91	93

cover appears to be delayed until May. The most significant correlation with latest Julian date, which usually falls in March, occurred for the April 100-cm soil temperature. The overall low significance of the correlation with latest date indicates that the latest Julian date has little influence on spring soil temperature. A meaningful correlation (92%) for the April 100-cm temperature was probably obtained because 50% of the latest Julian dates occurred at the end of the general winter snow cover. Apparently, isolated snowfalls that occur well beyond the general winter snow cover have little effect on either the monthly average of the quickly responding 10-cm soil temperature or on the more damped temperature fluctuations at 100 and 305 cm.

Correlations of less than 90% significance between air temperature and snow cover were found for all cases tested. The correlations of greatest significance, those between annual and May air temperatures and total days of snow cover (88% and 84% significance levels, respectively), are probably only as high as they are because local snow cover tends to be related to regional continental-scale snow cover. The snow cover on either scale may affect winter and spring regional-scale weather patterns, which in turn would tend to affect spring air temperatures. Clearly, local snow cover exhibits little influence on spring air temperatures. Local snow-cover parameters have been shown to affect local winter air temperature (Wayner 1973; Kukla 1981; Walsh et al. 1982), but this was not investigated as part of the present study.

As was expected, this study showed that for soil temperatures, more cases of correlations of high significance occur for longest duration of snow cover than for total number of days with an inch or more of snow cover. Significant correlations at all three of the soil depths chosen occur only for May for total days of snow cover, but for April and May for longest duration of snow cover. Longest durations of snow cover much shorter or much longer than normal expose or insulate, respectively, the surface to or from solar irradiation and air temperature, thereby affecting soil temperatures. Longest duration of snow cover is, therefore, a potential predictor of spring soil temperature. Significance probabilities for longest duration of snow cover are generally greatest in May. Because the annual soil temperature averages are affected by parts of two winters, total days of snow cover and longest duration of snow cover are equally sensitive predictors of annual soil temperature.

In summary, the soil temperature at the depths studied is most highly correlated with the longest duration of snow cover of the previous winter, particularly for May soil temperatures. Annual soil temperatures correlate well with both longest duration of snow cover and total days of snow cover, indicating a possible cause or effect relationship between snow cover and regional- and/or continental-scale weather patterns. Air temperature is correlated with total days of snow cover, but at significance probabilities below 90%. The 10° C Julian date is significantly correlated with snow cover only at 100 cm and is more highly correlated with longest duration of snow cover than with total days of snow cover. It may be possible to predict spring monthly and annual soil temperatures and 10° C date at 100 cm by using snow cover data from the previous winter. It does not appear, however, that predictions of annual and monthly air temperatures or 10° C date at 10 and 305 cm can be made using this snow cover data.

References

Foster, J., M. Owe, and A. Rango, 1982: Snow cover and temperature relationships in North America and Eurasia, J. of Climate and Appl. Meteorol. 22, 460-469.

Hess, P. E., 1976: Processing Argonne weather data, Radiological and Environmental Research Division Annual Report, ANL-76-88, Part IV, Argonne National Laboratory, pp. 140-152.

Kukla, G., 1981: Glaciological data. Report GD-11, National Oceanic and Atmospheric Administration, pp. 27-39.

Moses, H. and M. A. Bogner, 1967: Fifteen-year Climatological Summary: January 1, 1950 - December 1, 1964, ANL-7084, Argonne National Laboratory, 671 pp.

Wagner, J. A., 1973: The influence of average snow depth on monthly mean temperature anomaly, Mon. Wea. Rev. 101, 624-626.

Walsh, J. E., D. R. Tucek, and M. R. Peterson, 1982: Seasonal snow cover and short-term climatic fluctuations over the United States, Mon. Wea. Rev. 110, 1474-1485.

PUBLICATIONS BY THE STAFF OF THE ATMOSPHERIC PHYSICS PROGRAM FOR THE PERIOD JANUARY-DECEMBER 1983

Journal Articles and Book Chapters

D. L. Drapcho, D. L. Sisterson, and R. Kumar
NITROGEN FIXATION BY LIGHTNING ACTIVITY IN A THUNDERSTORM
J. Atmos. Environ. 17(4), 729-734

In-Young Lee
FORMATION OF SULFATE IN A CLOUD-FREE ENVIRONMENT
J. Climate and Applied Meteorology 22, 163-170

In-Young Lee
SIMULATION OF TRANSPORT AND REMOVAL PROCESSES OF THE SAHARAN DUST
J. Climate and Applied Meteorology 22, 632-639

C. M. Sheih, S. A. Johnson, and F. T. DePaul
CASE STUDIES OF AEROSOL SIZE DISTRIBUTION AND CHEMISTRY DURING PASSAGES OF A COLD AND WARM FRONT
Atmos. Environ. 17, 1299-1306

C. M. Sheih
A REPLY TO MOORE'S COMMENTS ON "CASE STUDIES OF AEROSOL SIZE DISTRIBUTION AND CHEMISTRY DURING PASSAGES OF A COLD AND WARM FRONT"
Atmos. Environ. 17, 1602-1603

D. L. Sisterson, B. B. Hicks, R. L. Coulter, and M. L. Wesely
DIFFICULTIES IN USING POWER LAWS FOR WIND ENERGY ASSESSMENT,
Solar Energy 31, 201-204

D. G. Streets, D. A. Knudson, and J. D. Shannon
SELECTED STRATEGIES TO REDUCE ACIDIC DEPOSITION IN THE UNITED STATES
Environmental Science & Technol. 17, 474-485A

M. L. Wesely and D. H. Stedman
AUTHORS' REPLY To "An Eddy-Correlation Measurement to NO_2 Flux to Vegetation and Comparison to O_3 Flux"
Atmos. Environ. 17, 1600

M. L. Wesely, D. R. Cook, and R. L. Hart
FLUXES OF GASES AND PARTICLES ABOVE A DECIDUOUS FOREST IN WINTERTIME
Boundary-Layer Meteorol. 27, 237-255

M. L. Wesely
TURBULENCE TRANSPORT OF OZONE TO SURFACES COMMON IN THE EASTERN HALF OF THE UNITED STATES
In: Trace Atmospheric Constituents: Properties, Transformation, and Fates, Advances in Science and Technology, Vol. 12, Chapter 8 (S. E. Schwartz, ed.) Wiley, NY, 345-370

Conference Proceedings and Miscellaneous Reports

R. E. Boers, E. Eloranta, W. P. Hooper, and R. L. Coulter
LIDAR MEASUREMENTS OF THE INTERGRATED KINETIC ENERGY BUDGET.
Proceedings, Sixth Symposium on Turbulence and Diffusion, March 22-25, 1983, Boston, MA, 205-206

R. E. Boers, E. W. Eloranta, and R. L. Coulter
LIDAR MEASUREMENTS OF THE ATMOSPHERIC ENTRAINMENT ZONE
Proceedings, Sixth Symposium on Turbulence and Diffusion, March 22-25, 1983, Boston, MA, 227-228

R. L. Coulter and T. J. Martin
REMOTE SENSING OF WINDS AND TURBULENCE ABOVE COMPLEX TERRAIN DURING ASCOT-1980
ANL/ER-83-1, ASCOT-83-4, Environmental Research Division, Argonne National Laboratory, Prepared for ASCOT Program, Office of Health and Environmental Research, U. S. Department of Energy.

R. L. Coulter and M. L. Wesely
METEOROLOGICAL AND POLLUTANT PROFILES UNDER VERY STABLE CONDITIONS
Proceedings, Sixth Symposium on Turbulence and Diffusion, March 22-25, 1983, Boston, MA, 294-296

J. L. Durham, B. B. Hicks, M. L. Wesely, R. G. DePena, and D. Thomson
STATUS OF RESEARCH TO DEVELOP ACIDIC DRY DEPOSITION MONITORING CAPABILITY
Preprint Volume, 76th Annual Meeting of the Air Pollution Control Association, June 19-24, 1983, Atlanta, GA, 1-8

P. Frenzen and R. L. Hart
A FURTHER NOTE ON THE KOLMOGOROV-VON KARMAN PRODUCT AND THE VALUES OF THE CONSTANTS
Proceeding, Sixth Symposium on Turbulence and Diffusion, March 22-25, 1983, Boston, MA, 24-27

P. Frenzen
ON THE ROLE OF FLUX DIVERGENCE TERMS IN THE TURBULENT ENERGY EQUATION
Proceeding, Sixth Symposium on Turbulence and Diffusion, March 22-25, 1983, Boston, MA, 305-308

B. B. Hicks, M. L. Wesely, R. L. Coulter, R. L. Hart, J. L. Durham, R. Speer, and D. H. Stedman
AN EXPERIMENTAL STUDY OF SULFUR DEPOSITION TO GRASSLAND
In: Precipitation Scavenging, Dry Deposition, and Resuspension, Vol. 2 (H. R. Pruppacher, R. G. Semonin, and W. G. N. Slinn, eds.), Elsevier, NY, 933-942

A. J. Policastro
EVALUATION OF SELECTED MODELS
In: An Evaluation of Effluent Dispersion and Fate Models for OCS Platforms, Vol. 1: Summary and Recommendations, Proceedings of the Workshop, February 7-10, 1983, Santa Barbara, CA, Sponsored by Minerals Management Service, U.S. Department of the Interior, 33-48

C. M. Sheih, S. A. Johnson, and F. T. DePaul
A CASE STUDY OF AEROSOL SIZE DISTRIBUTION AND CHEMISTRY DURING PASSAGES OF A COLD AND A WARM FRONT
Fourth International Conference on Precipitation Scavenging, Dry Deposition and Resuspension, Vol. 1, November 29 - December 3, 1982, Santa Monica, CA, pp. 323-332

C. M. Sheih, P. Frenzen, and R. L. Coulter
ON THE MEASUREMENT OF SUBGRID-SCALE EDDY DIFFUSIVITY
Sixth Symposium on Turbulence and Diffusion, March 22-25, 1983, Boston, MA, 253-254

D. L. Sisterson, M. L. Wesely, R. L. Coulter, R. L. Hart, T. Yamada, B. B. Hicks, P. E. Hess, D. R. Cook, J. D. Shannon, and G. A. Zerbe
THE RUSH FIELD EXPERIMENTS: GROWTH AND INITIAL DECAY OF THE MIXED LAYER OVER AN AUTUMN LANDSCAPE
ANL/RER-83-1, Radiological and Environmental Research Division, Argonne National Laboratory, 81 pp.

M. L. Wesely, D. R. Cook, R. L. Hart, B. B. Hicks, J. L. Durham, R. Speer, D. H. Stedman, and R. J. Tropp
EDDY-CORRELATION MEASUREMENTS OF THE DRY DEPOSITION OF PARTICULATE SULFUR AND SUBMICRON PARTICLES
In: Precipitation Scavenging, Dry Deposition, and Resuspension, Vol. 2 (H. R. Pruppacher, R. G. Semonin, and W. G. N. Slinn, eds.), Elsevier, NY, 943-952

Distribution for ANL-83-100 Part IV

Internal:

A. Schriesheim
H. Drucker
E. G. Pewitt
K. L. Brubaker
L. A. Chapman (5)
D. R. Cook
R. L. Coulter
E. J. Croke
F. T. DePaul
J. D. DePue
A. J. Dvorak
P. Failla
P. Frenzen
P. F. Gustafson
R. L. Hart
P. E. Hess
B. D. Holt
E. Huberman
M. Inokuti
S. A. Johnson
R. Kumar
I-Y. Lee
B. M. Lesht
T. J. Martin
R. D. Olsen
A. J. Policastro
J. J. Roberts
D. M. Rote
J. D. Shannon
C. M. Sheih
D. L. Sisterson
R. W. Springer
C. M. Stevens
D. G. Streets
M. L. Wesely
APP/ER Library (100)
A. B. Krisciunas
ANL Patent Dept.
ANL Contract File
ANL Libraries (2)
TIS Files (6)

External:

DOE-TIC, for distribution per UC-11 (212)
Manager, Chicago Operations Office, DOE
Environmental Research Division Review Committee:
J. W. Firor, National Center for Atmospheric Research, Boulder
D. W. Moeller, Harvard School of Public Health
R. A. Reck, General Motors Research Lab.
P. G. Risser, Illinois Natural History Survey, Champaign
D. W. Thomson, Pennsylvania State U.
R. E. Wildung, Battelle Pacific Northwest Lab.
B. Ackerman, Illinois State Water Survey, Champaign
W. C. Ackermann, U. Illinois, Urbana
E. Adams, Massachusetts Inst. Technology
Air Pollution Control Association, Library, Pittsburgh
L. H. Allen, Jr., U. Florida
A. W. Andren, U. Wisconsin, Madison
R. A. Anthes, National Center for Atmospheric Research, Boulder
S. P. S. Arya, North Carolina State U.
D. Atlas, NASA Goddard Space Flight Center
Atmospheric Sciences Lab., White Sands Missile Range
E. J. Aubert, NOAA, Ann Arbor
S. I. Auerbach, Oak Ridge National Lab.
F. I. Badgley, U. Washington
R. H. Ball, Div. Environmental Issues, USDOE
D. S. Ballantine, Office of Health and Environmental Research, USDOE
M. L. Barad, Belmont, Mass.
S. Barr, Los Alamos National Lab.
S. Berman, State U. College at Oneonta, N. Y.
C. Bhumralker, SRI International, Menlo Park
E. Bierly, National Science Foundation
G. E. Birchfield, Northwestern U.
S. Booras, Illinois Inst. for Environmental Quality, Chicago
R. D. Bornstein, San Jose State U.
L. Botts, Northwestern U.
R. R. Braham, Jr., U. Chicago
S. D. Burks, Naval Environmental Prediction Research Facility, Monterey

J. A. Businger, National Center for Atmospheric Research, Boulder
S. H. Cadle, General Motors Research Labs.
California, U. of, Los Angeles, Chairman, Dept. of Meteorology
G. S. Campbell, Washington State U.
G. R. Carmichael, U. Iowa
H. Cember, Northwestern U.
J. E. Cermak, Colorado State U.
J. Chang, National Center for Atmospheric Research, Boulder
S. A. Changnon, Illinois State Water Survey, Champaign
R. J. Charlson, U. Washington
N. Chen, ATDL/NOAA, Oak Ridge
J. Ching, USEPA, Research Triangle Park
D. P. Chock, General Motors Corp., Warren, Mich.
R. M. Cionco, Atmospheric Science Lab., White Sands Missile Range
T. L. Clark, USEPA, Research Triangle Park
W. E. Clements, Los Alamos National Lab.
Colorado State U., Library, Dept. of Atmospheric Sciences
Commonwealth Edison Co., Dept. of Environmental Planning, Chicago
Connecticut, U. of, Chairman, Dept. of Meteorology
Cornell U., Agricultural Experiment Station, Geneva
Cornell U., Librarian, Microclimatology Research Unit
R. B. Corotis, Johns Hopkins U.
S. Corrsin, Johns Hopkins U.
E. B. Cowling, North Carolina State U.
T. V. Crawford, Savannah River Lab.
C. T. Csanady, Woods Hole Oceanographic Inst.
R. C. Dahlman, Office of Basic Energy Sciences, USDOE
K. L. Davidson, U. S. Naval Postgraduate School
D. Davis, Georgia Inst. Technology
J. W. Deardorff, Oregon State U.
K. Demerjian, USEPA, Research Triangle Park
R. Dennis, USEPA, Research Triangle Park
R. DePena, Pennsylvania State U.
M. Dickerson, Lawrence Livermore National Lab.
C. R. Dickson, NOAA, Idaho Falls
R. R. Draxler, Air Resources Labs., NOAA, Rockville
J. Droppo, Battelle Pacific Northwest Lab.
R. A. Duce, U. Rhode Island
Duke U., Chairman, Dept. of Environmental Science
J. L. Durham, USEPA, Research Triangle Park
A. Eddy, U. Oklahoma
C. Elderkin, Battelle Pacific Northwest Lab.
W. P. Elliott, NOAA, Silver Spring
E. Eloranta, U. Wisconsin, Madison
G. H. Fichtl, NASA Marshall Space Flight Center
R. G. Fleagle, U. Washington
S. Friedlander, California Inst. Technology
C. A. Friehe, U. California, Irvine
J. Friend, Drexel U.
J. Galloway, U. Virginia
A. A. Garrett, Savannah River Lab.
D. M. Gates, U. Michigan
D. F. Gatz, Illinois State Water Survey, Champaign
N. Gillani, Washington U.

J. C. Golden, Jr., Commonwealth Edison Co., Chicago
J. Goll, U. S. Minerals Management Service, Reston
W. Gray, Colorado State U.
T. J. Gross, Office of Basic Energy Sciences, USDOE
P. H. Gudiksen, Lawrence Livermore National Lab.
C. Hakkarinan, Electric Power Research Inst., Palo Alto
J. M. Hales, Battelle Pacific Northwest Lab.
F. F. Hall, NOAA, Boulder
S. R. Hanna, ERT, Inc., Concord, Mass.
Harvard U., Chairman, Dept. of Meteorology
D. A. Haugen, Wave Propagation Lab., NOAA, Boulder
Hawaii, U. of, Chairman, Dept. of Meteorology
J. L. Heffter, Air Resources Lab., NOAA, Rockville
B. B. Hicks, ATDL/NOAA, Oak Ridge
G. M. Hidy, Desert Research Inst., Reno
G. Hilst, Electric Power Research Inst.
W. Hooke, Wave Propagation Lab., NOAA, Boulder
T. W. Horst, Battelle Pacific Northwest Lab.
R. P. Hosker, Jr., ATDL/NOAA, Oak Ridge
A. H. Huber, USEPA, Research Triangle Park
R. B. Husar, Washington U.
IIT Research Institute, Document Library
Illinois Environmental Protection Agency, Manager, Div. of Air Pollution Control, Springfield
Illinois State Water Survey, Librarian, Champaign
Illinois, U. of, Chicago Circle Campus, Library
Iowa State U., Chairman, Dept. of Meteorology
J. Jansen, Southern Company Services, Inc., Birmingham
W. B. Johnson, SRI International, Menlo Park
J. C. Kaimal, Wave Propagation Lab., NOAA, Boulder
E. Klappenbach, USEPA, Chicago
H. Klieforth, Desert Research Inst., Reno
J. B. Knox, Lawrence Livermore National Lab.
C. W. Kreitzburg, Drexel U.
S. V. Krupa, U. Minnesota
H. H. Lettau, U. Wisconsin, Madison
D. K. Lilly, U. Oklahoma
M. K. Liu, Systems Applications, Inc., San Rafael
F. L. Ludwig, Stanford Research Inst.
W. A. Lyons, Mesomet, Inc., Chicago
M. C. MacCracken, Lawrence Livermore National Lab.
W. M. Mach, Florida State U.
J. Mahlman, Princeton U.
L. Marht, Oregon State U.
E. H. Markee, Office of Nuclear Regulatory Research, USNRC
E. A. Martell, National Center for Atmospheric Research, Boulder
Maryland, U. of, Chairman, Dept. of Engineering
D. J. McNaughton, TRC Environmental Consultants, Inc., Salt Lake City
G. Mellor, Princeton U.
R. Meroney, Colorado State U.
R. Meyers, Atmospheric Science Lab., White Sands Missile Range
Miami, U. of, Inst. of Atmospheric Science, Coral Gables
P. Michael, Brookhaven National Lab. (3)
Michigan, U. of, Great Lakes Research Div.

R. W. Miksad, U. Texas, Austin
E. Miller, Corvallis, Ore.
J. M. Miller, Air Resources Lab., NOAA, Rockville
T. A. Miskimen, American Electric Power Service Corp., New York City
Missouri, U. of, Chairman, Dept. of Atmospheric Science, Columbia
Missouri, U. of, Chairman, Dept. of Meteorology, Rolla
K. Miyakado, Princeton U.
V. A. Mohnen, SUNY at Albany
E. L. Molle-Christensen, Massachusetts Inst. Technology
C. H. Mortimer, U. Wisconsin, Milwaukee
H. Moses, Office of Health and Environmental Research, USDOE
P. K. Mueller, Electric Power Research Inst., Palo Alto
T. J. Murphy, DePaul U.
C. J. Nappo, Jr., NOAA, Oak Ridge
NASA Goddard Space Flight Center, Librarian
NASA Langley Research Center, Technical Library
NASA Lewis Research Center, Librarian
National Center for Atmospheric Research, Library, Boulder
National Oceanic and Atmospheric Admin., Library, Silver Spring
National Weather Service, Headquarters, Silver Spring
W. D. Neff, Environmental Research Lab., Boulder
Nevada, U. of, Desert Research Inst.
R. E. Newell, Massachusetts Inst. Technology
L. Newman, Brookhaven National Lab.
New York, City U. of, Chairman, Dept. of Meteorology
G. Nichols, Jr., Manchester, Mass.
E. C. Nickerson, NOAA, Boulder
K. Noll, Illinois Inst. Technology
Northwestern U., Library, The Technical Institute
V. E. Noshkin, Lawrence Livermore National Lab.
Notre Dame, U. of, Library, Dept. of Meteorology
H. T. Odum, U. Florida
Y. Ogura, U. Illinois, Urbana
Oklahoma, U. of, Chairman, Dept. of Meteorology
R. E. Orville, SUNY at Albany
W. S. Osburn, Office of Health and Environmental Research, USDOE
H. G. Ostlund, U. Miami, Fla.
W. Ott, USEPA, Rockville
D. H. Pack, McLean, Va.
H. A. Panofsky, San Diego
D. Pashayan, USEPA, Washington
C. A. Paulson, Oregon State U.
W. Pennell, Battelle Pacific Northwest Lab.
L. K. Peters, U. Kentucky
J. H. Phillips, USEPA, Chicago
R. A. Pielke, Colorado State U.
G. W. Platzman, U. Chicago
J. M. Prospero, Rosensthiel School of Marine and Atmospheric Science, Miami
W. O. Pruitt, U. California, Davis
H. R. Pruppacher, U. California, Los Angeles
R. A. Ragotzkie, U. Wisconsin, Madison
D. Randerson, Air Resources Lab., NOAA, Las Vegas
S. Rao, ATDL/NOAA, Oak Ridge
D. E. Reichle, Oak Ridge National Lab.

W. E. Reifsnyder, Yale School of Forestry and Environmental Studies
E. R. Reiter, Colorado State U.
Rhode Island, U. of, Chairman, Dept. of Environmental Science
J. Robbins, U. Michigan
E. Robinson, Washington State U.
G. D. Robinson, Center for the Environment and Man, Hartford, Conn.
N. J. Rosenberg, U. Nebraska
E. Ryznar, U. Michigan
P. Samson, U. Michigan
W. Saucier, North Carolina State U.
J. H. Saylor, NOAA, Great Lakes ERL, Ann Arbor
C. L. Schelske, U. Michigan
F. A. Schiermier, USEPA, Research Triangle Park
J. F. Schubert, Savannah River Lab.
S. Schwartz, Brookhaven National Lab.
R. Semonin, Illinois State Water Survey, Champaign
R. J. Serafin, National Center for Atmospheric Research, Boulder
S. SethuRaman, North Carolina State U.
J. Shinn, Lawrence Livermore National Lab.
H. Sievering, Governors State U., University Park, Ill.
D. H. Slade, Office of Health and Environmental Research, USDOE
W. H. Snyder, USEPA, Research Triangle Park
K. C. Spengler, American Meteorological Society, Boston
C. Spicer, Battelle Columbus Lab.
G. E. Start, NOAA, Idaho Falls
C. R. Stearns, U. Wisconsin, Madison
E. F. Stoermer, U. Michigan
R. H. Strange II, National Science Foundation
R. B. Stull, U. Wisconsin, Madison
C. B. Tanner, U. Wisconsin, Madison
Tennessee, U. of, Chairman, Dept. of Meteorology
Texas A&M U., Librarian, Dept. of Oceanography and Meteorology
Texas, U. of, Atmospheric Science Group, Austin
D. W. Thomson, Pennsylvania State U.
K. H. Underwood, Zontech, Inc., Van Nuys
U. S. Dept. of Agriculture, Library, Washington
U. S. Dept. of the Interior, Bu. of Reclamation, Denver
U. S. Dept. of the Interior, Library, Washington
U. S. Dept. of Transportation, Librarian, Transportation Systems Center, Cambridge, Mass.
U. S. Dept. of Transportation, Library, Washington
U. S. Environmental Protection Agency, Nat. Envtl. Res. Ctr., Cincinnati
U. S. Naval Postgraduate School, Chairman, Dept. of Meteorology
I. Van der Hoven, NOAA, Silver Spring
W. M. Vaughan, EMI, University City, Mo.
S. B. Verma, U. Nebraska, Lincoln
H. L. Volchok, Environmental Measurements Lab., USDOE, New York City
J. A. Warburton, Desert Research Inst., Reno
H. Weaver, U. S. Geological Survey, Denver
J. A. Weinman, U. Wisconsin, Madison
L. L. Wendell, Battelle Pacific Northwest Lab.
R. E. Wildung, Battelle Pacific Northwest Lab.
M. H. Wilkening, New Mexico Inst. of Mining and Technology, Socorro
J. C. Willett, Naval Research Lab.

J. C. Wilson, U. Minnesota
W. E. Wilson, National Center for Air Pollution Control, USEPA, Research Triangle Park
J. W. Winchester, Florida State U.
Woods Hole Oceanographic Institution, Document Library
J. C. Wyngaard, National Center for Atmospheric Research, Boulder
Wyoming, U. of, Dept. of Atmospheric Resources
Yale U., Chairman, Dept. of Geology and Geophysics
T. Yamada, Los Alamos National Lab.
R. Yamartino, Environmental Research and Technology, Inc., Concord, Mass.
J. Young, U. Wisconsin, Madison
H. Zar, USEPA, Chicago
K. Zar, U. Chicago
E. F. Bradley, C.S.I.R.O., Canberra, Australia
C.S.I.R.O., Div. of Atmospheric Physics, Librarian, Mordialloc, Australia
C.S.I.R.O., Div. of Environmental Mechanics, Librarian, Canberra, Australia
Commonwealth Meteorology Research Centre, Librarian, Melbourne, Australia
J. R. Garratt, C.S.I.R.O., Mordialloc, Australia
G. D. Hess, Environmental Protection Authority of Victoria, East Melbourne, Australia
G. Lorimer, Chisholm Inst. Technology, Victoria, Australia
Melbourne, U. of, Librarian, RAAF Academy/Physics Dept., Australia
J. R. Philip, C.S.I.R.O., Canberra, Australia
P. Schwerdtfeger, Flinders U. of South Australia, Bedford Park, Australia
N. A. Shaw, Footscray Inst. Technology, Footscray, Australia
S. Turner, Australian National University, Sutherland
Canada Centre for Inland Waters, Librarian, Burlington
F. Elder, Canada Centre for Inland Waters, Burlington
J. Gannon, International Joint Commission, Windsor, Canada
K. D. Hage, U. Alberta, Edmonton, Canada
D. N. Kirshak, Ontario Hydro, Toronto, Canada
H. C. Martin, Atmospheric Environment Service, Downsview, Canada
McGill U., Chairman, Dept. of Meteorology, Montreal, Canada
W. J. Moroz, Ontario Hydro, Toronto, Canada
R. E. Munn, U. Toronto, Canada
T. R. Oke, U. British Columbia, Vancouver, Canada
L. Shenfeld, Ministry of the Environment, Toronto, Canada
P. A. Taylor, Atmospheric Environment Service, Downsview, Canada
G. W. Thurtell, Guelph, Canada
Toronto, U. of, Library, Serials Dept., Canada
T. Turner, Atmospheric Environment Service, Downsview, Canada
E. Voldner, Atmospheric Environment Service, Downsview, Canada
R. A. Vollenweider, Canada Centre for Inland Waters, Burlington
D. M. Whelpdale, Atmospheric Environment Service, Downsview, Canada
C-Y. Tseng, Inst. of Physics, Nankang, Taiwan, China
M-Y. Chou, Academia Sinica, Beijing, People's Republic of China
X-F. Zhang, Academia Sinica, Beijing, People's Republic of China
N. E. Busch, Danish AEC, Risø
L. Kristenson, Risø National Lab., Roskilde, Denmark
L. Prahm, Risø National Lab., Roskilde, Denmark
A. C. Chamberlain, UKAEA, Harwell, England
J. Garland, AERE, Harwell, England
Inst. of Oceanographic Sciences, Librarian, Wormley, England
P. Liss, U. East Anglia, Norwich, England

Meteorological Office Library, Bracknell, England
F. B. Smith, Meteorological Office, Bracknell, England
P. A. Taylor, U. Southampton, England
L. Hasse, Institut für Meerskunde, Kiel, Germany
W. Klug, Technische Hochschule Darmstadt, Germany
D. Lege, U. Hannover, Germany
Meteorologisches Inst. der Universitat Hamburg, Librarian, Germany
K. O. Munnich, Physikalische Inst. der Universitat Heidelberg, Germany
R. Roth, Technischen Universitat Hannover, Germany
Y. Neumann, U. Jerusalem, Israel
O. Vittori, Laboratorio Microfisica dell' Atmosfera, Bologna, Italy
E. Inoue, National Inst. of Agricultural Sciences, Tokyo, Japan
K. Sahashi, Okayama U., Japan
H. Tennekes, Royal Netherlands Meteorological Inst., Debilt
R. M. van Aalst, TNO, Delft, The Netherlands
K. G. McNaughton, Dept. of Scientific and Industrial Research, Palmerston North, New Zealand
A. Eliassen, Norwegian Meteorological Inst., Oslo
D. T. Gjessing, Norwegian Defense Research Establishment, Kjeller
L. Granat, U. Stockholm, Sweden
Swedish Meteorological and Hydrological Inst., Norrköping
Academy of Sciences of the USSR, Librarian, Inst. of Atmospheric Physics, Moscow